NASA TECHNICAL NOTE

NASA TN D-3984

NASA TN D-3984
C.1

Correcte Copy

OPTICAL AND MICROWAVE COMMUNICATIONS -

A COMPARISON

by F. Kalil

Goddard Space Flight Center
Greenbelt, Md.

NATIONAL AERONAUTICS AND SPACE ADMINISTRATION • WASHINGTON, D. C. • MAY 1968

NASA TN D-3984

OPTICAL AND MICROWAVE COMMUNICATIONS—

A COMPARISON

By F. Kalil

Goddard Space Flight Center
Greenbelt, Md.

NATIONAL AERONAUTICS AND SPACE ADMINISTRATION

For sale by the Clearinghouse for Federal Scientific and Technical Information
Springfield, Virginia 22151 – CFSTI price $3.00

ABSTRACT

Some preliminary comparisons are made of microwave, millimeter, and optical communication systems for space communication from a spacecraft at Mars distances. An attempt is made to be realistic with regard to technology. Some discussion of thermal, quantum, and sky noise is included, as well as some discussion and analyses of microwave, millimeter wave, and optical technology; acquisition and tracking; and some mission analysis. Based on the considerations herein, it appears likely that in the radio spectrum, the S-Band is the better place to operate. However, it also appears likely that optical communication systems have the greater potential for higher data rates—up to about 10^8 bps at Mars distances. Table 9 summarizes the results.

CONTENTS

Abstract ii

INTRODUCTION 1

ANALYSIS 1

Range Equation 1

Noise 2

Microwave and Millimeter Systems 5

Optical Systems 9

Mission Analysis 20

SUMMARY 29

References 31

Appendix A—Noise Figure and Effective Noise Temperature 35

Appendix B—The Point Ahead Angle 39

OPTICAL AND MICROWAVE COMMUNICATIONS– A COMPARISON*

by
F. Kalil
Goddard Space Flight Center

INTRODUCTION

A comparison of lasers versus microwaves and millimeter waves in space communications has been reported in the literature by S. Gubin, R. S. Marsten, and D. Silverman. However, in that study (Reference 1), a laser diffraction limited beamwidth of 20 arc seconds was assumed. Primarily because of this large beamwidth, the laser communication systems did not compare favorably with the microwave system. Furthermore, the best available laser source was not considered in Reference 1, namely, the 130 watt, cw, 10.6 μ wavelength, CO_2 laser with an excellent efficiency of approximately 13 percent, developed by Bell Telephone Laboratories (see Reference 2). The largest cw laser source they considered was a 2w ionized argon gas laser at 0.4880 μ wavelength; in the microwave region, they only considered S-Band, 10 GHz, and 25 GHz systems.

In this paper, similar comparisons will be made using more up-to-date values for cw laser output powers of 4w and 130w (see Reference 2), and laser diffraction limited beamwidths of 1 arc second. This is a factor of 10 larger than the present goal of 0.1 arc second diffraction limited beamwidth (see Reference 3) being emphasized in the research programs sponsored by the Office of Advanced Research and Technology, NASA Headquarters, and by the NASA Electronics Research Center (see Reference 4).

ANALYSIS

In the following analysis, the simple range equation will be used to evaluate the maximum amount of data (bits/sec) which can be transmitted to the earth from a spacecraft at Mars distances with various communication systems. The distance chosen for this analysis was 1.852×10^8 kilometers or 10^8 nautical miles.

Range Equation

The simple range equation is based on the following considerations. Assume that transmitting and receiving antennae are separated by a distance $R >> \lambda$ (wavelength), such that the received

*This publication replaces one of the same title and author, published June, 1967, which contained numerous serious typographical errors.

wavefront may be considered planar over the receiving antenna cross section. If the transmitter antenna were omnidirectional (isotopic radiator), then the inverse square law would be applicable; i.e., the transmitter power P_T' would be uniformly spread out over a sphere, so that the power per unit area at the receiver would be $P_T'/4\pi R^2$. However, if the transmitting antenna is directional with a directive gain of G_T, then the power per unit area at the receiver would be $G_T P_T'/4\pi R^2$, since by definition, the directive gain of an antenna is the ratio of the power received or radiated in a given direction to that which would be received or radiated if the antenna were nondirectional, and is given by

$$G = \frac{4\pi A_{eff}}{\lambda^2} , \tag{1}$$

where A_{eff} is the effective capture cross section of the antenna, and for circular apertures is taken to be about 0.54 A_R. Thus, the received power is

$$P_R' = \frac{P_T' G_T A_{R,eff}}{4\pi R^2} . \tag{2}$$

If one wishes to define P_R as the received power at the receiver input terminals, and P_T as the power output at the transmitter power amplifier terminals, then one must take account of the received and transmitter line losses L_R and L_T, in which case

$$P_R = \frac{P_T G_T A_{R,eff}}{4\pi R^2 L_T L_R} . \tag{3}$$

Noise

The received carrier signal-to-noise ratio is

$$\frac{C}{N} = \frac{P_T G_T A_{R,eff}}{4\pi R^2 L_T L_R N} , \tag{4}$$

where N is the total noise at the receiver input terminals and is given by

$$N = \psi B , \tag{5}$$

where ψ is the noise power density, and B is the effective detection bandwidth. This has been extensively treated in References 5 through 9. In Reference 5 (see also Reference 1), B. M. Oliver has shown that the total noise power density of an ideal amplifier is given by

$$\psi_n = \frac{hf}{e^{hf/kT} - 1} + hf , \tag{6}$$

where T is the effective noise temperature in degrees Kelvin at the input, $h = 6.624 \times 10^{-34}$ watt-sec^2 is Planck's constant, $k = 1.38047 \times 10^{-23}$ watt-sec-deg^{-1} is Boltzmann's constant, and f is the frequency in cycles per sec. Similarly, the total noise power density of an ideal linear amplitude detector or phase detector is

$$\psi_a = \frac{hf}{e^{hf/kT} - 1} + \frac{hf}{2} \quad . \tag{7}$$

An ideal amplifier or detector is "noiseless"; i.e. the signal-to-noise ratio is the same at its output terminals as at its input terminals. In terms of noise factor (or noise figure as it is sometimes called), a noiseless amplifier, detector, or network in general, has a noise figure of unity. A more thorough and detailed discussion of noise figure and noise temperature is given in Appendix A. Furthermore, in subsequent sections of this report, it will become clear as to how a nonideal amplifier or detector could be analyzed with the aid of the foregoing considerations.

It should be noted that in the case of a noncoherent power detector such as a photodetector which is not used as a mixer, then the right-hand term of Equation 7 becomes 2hf (References 5 and 10).

The first term on the right-hand side of Equations 6 and 7 is the thermal noise caused by thermal agitation of the molecules or electric charge in the equivalent resistive element of the circuit (see References 8 and 9). The second term on the right-hand side of these equations is the quantum noise which is the result of the well established and experimentally verified principles of quantum mechanics, namely:

1. The intensity of a radiation field, i.e., the product of its amplitude vector by the complex conjugate of its amplitude vector, specifies the probability of intercepting a photon. Therefore, even if the received radiation is a coherent monochromatic wave of constant power P, photons will be received in a random fashion.

2. The Heisenberg Uncertainty Principle states that two canonically conjugate variables cannot be determined precisely simultaneously. In particular,

$$\Delta E \, \Delta t \geq \frac{h}{4\pi} \quad , \tag{8}$$

where $E = hf$ is the photon energy, hence ΔE is the uncertainty in photon energy, and Δt is the uncertainty in the time of arrival of the photon. The physical essence of Equation 8 is that the more precisely the photon energy is known, the less precise its time of arrival can be determined. Basically, it is this uncertainty in time of arrival of the photons which causes the quantum noise being referred to here.

To facilitate plotting Equations 6 and 7, we divide through by kT and plot ψ/kT as a function of hf/kT as shown in Figure 1. This figure shows how the thermal, quantum, and total noise vary with

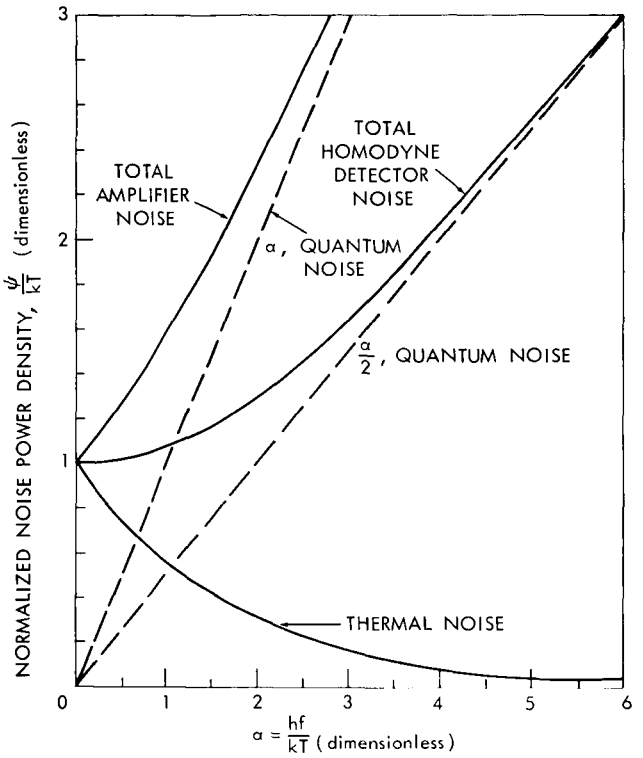

Figure 1—Comparison of thermal, quantum, and total noise power density.

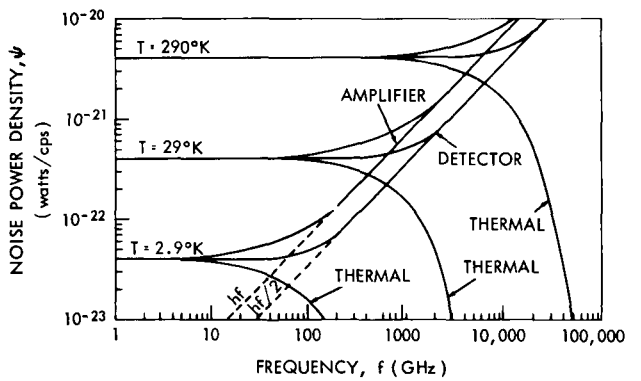

Figure 2—Thermal, quantum, and total noise power density as a function of frequency at various temperatures.

hf/kT, and how they compare with each other. It can be seen that at

$$\alpha = \frac{hf}{kT} << 1 ,$$

or $hf << kT$, then the thermal noise predominates, and the detector is said to be thermal noise limited; while at

$$\alpha = \frac{hf}{kT} >> 1 ,$$

or $hf >> kT$, the quantum noise predominates, and the detector is said to be quantum noise limited. Thus there are two regions in the noise spectrum.

1. When $hf < kT$, in which case $\psi \approx kT$ which is the familiar expression for noise density.

2. When $hf > kT$, in which case $\psi_a \cong hf$ for an ideal amplifier and coherent heterodyne detection, while $\psi_d \approx hf/2$ for an ideal linear amplitude or phase detector or coherent homodyne detection, and in the case of noncoherent power detection, $\psi_d \approx 2hf$.

Shown in Figure 2 is the noise power density as a function of frequency f for various temperatures T. It can be seen from this figure that the thermal noise drops off sharply with increased frequency after hf begins to become significantly larger than kT.

It can be seen from Figures 1 and 2 that if thermal noise were the only noise present, then the received signal power required for a given communication rate or a given signal-to-noise ratio would also decrease rapidly. Thus, by choosing the carrier frequency high enough, one might falsely conclude that it would be possible to receive the entire contents of a book with a total received energy equivalent to one photon or less. The fact that this is not possible provides further evidence of the validity of the quantum mechanics principles and the existence of quantum noise.

Microwave and Millimeter Systems

In the case of microwave and millimeter systems wherein $kT >> hf$, the noise power density ψ becomes

$$\psi \approx kT , \tag{9}$$

where T is the effective noise temperature in degrees Kelvin at the input. Various noise sources can be included in the temperature T by equating them to an equivalent temperature and adding the effective temperatures contributed by each to get a total equivalent system noise temperature (refer to Appendix A for further details). In addition to the noise generated within the receiver, other noise sources include atmospheric attenuation, atmospheric noise, galactic noise, sidelobe noise, backlobe noise (in the case of a mesh type antenna), and "spill-over" noise (noise which enters the antenna input by optical paths other than via the lobes).

The resultant tropospheric contribution to the noise temperature of a narrow beam antenna the radiation pattern of which admits no sidelobes or backlobes is given by

$$T_{troposphere} = \int_0^\infty \alpha T \left[\exp \int_0^r \alpha \, dr \right] dr , \tag{10}$$

where α and T are the absorption coefficient (reciprocal length units) and temperature, respectively, at any point in the atmosphere at a distance r from the antenna. Shown in Figure 12-18 of Reference 10 are the calculated values of $T_{troposphere}$ versus frequency at various antenna beam elevation angles. These computed curves are in essential agreement with experimental measurements. Shown in Figure 8 of Reference 5 are some typical effective antenna temperatures which include the effects of cosmic noise for both quiet and noisy sky, atmospheric absorption for good and bad weather, and ground radiation scattered by rain or snow.

Using the foregoing information, the system capabilities for an S-Band system were computed and are tabulated in Table 1. The assumptions are all in the table, but some are repeated here. For example, the transmitter powers used were 20 watts (typical of the Apollo S/C* system) and 100 watts (projected future capability). The value of 100 watts for projected future capability may be conservative, since an 8-kw, cw, C-Band TWT (traveling wave tube) is now an off-the-shelf item (see Reference 11). Although this TWT operates in the C-Band, it is at least indicative of what might be in the offing at S-Band for future spaceborne applications. At the same time, however, it must be kept in mind that the necessary power supply may not be conducive for spaceborne use because of size and weight. It was for such reasons as this that the 100 watt spaceborne transmitter power was used in Table 1 as a future projected capability for a Mars mission.

Because of the atmospheric "windows" at about 16 GHz, 34 GHz, and 94 GHz (see Figure 3 in this report and Figure 12-17 of Reference 10), and the availability of S/C transmitter sources at these

*S/C = spacecraft.

Table 1

Analysis of Microwave Transmission from Mars Space Vehicle to Earth-Based Station for P_T = 20 w and 100 w.

Parameter	Values	
	P_T = 20 w	P_T = 100 w
Frequency	2.3 GHz	2.3 GHz
Wavelength	13 cm (0.428 ft)	13 cm (0.428 ft)
Range	1.852×10^8 km (10^8 nm)	1.852×10^8 km (10^8 nm)
Transmitter power, P_T	20 w 13.0 dbw	100 w 20.0 dbw
S/V antenna gain, G_T	4.88 m (16 ft) 38.8 db	4.88 m (16 ft) 38.8 db
S/V transmission loss	-0.5 db	-1.0 db
Free space path loss, $\lambda^2/(4\pi R)^2$	-265.1 db	-265.1 db
Ground antenna gain, G_R(1)	64 m (210 ft) 60.0 db	64 m (210 ft) 60.0 db
Receiver power, P_R	-153.8 dbw	-147.3 dbw
CNR = P_R/KTB	10.0 db	10.0 db
Allowable noise power	-163.8 dbw	-157.3 dbw
System noise temperature(2)	50°K -211.7 dbw/Hz	50°K -211.7 dbw/Hz
Noise bandwidth	61.5 kHz 47.9 db Hz	275 kHz 54.4 db Hz
Maximum transmission rate(3)	6.15×10^4 bits/sec	2.75×10^5 bits/sec

NOTES: (1) Including ground line loss (Reference 1).
(2) Includes 10°K receiver noise, 30 ± 10°K sky noise (i.e., over-all background noise from sky, spill-over, sidelobes, and backlobes).
(3) No margins included.

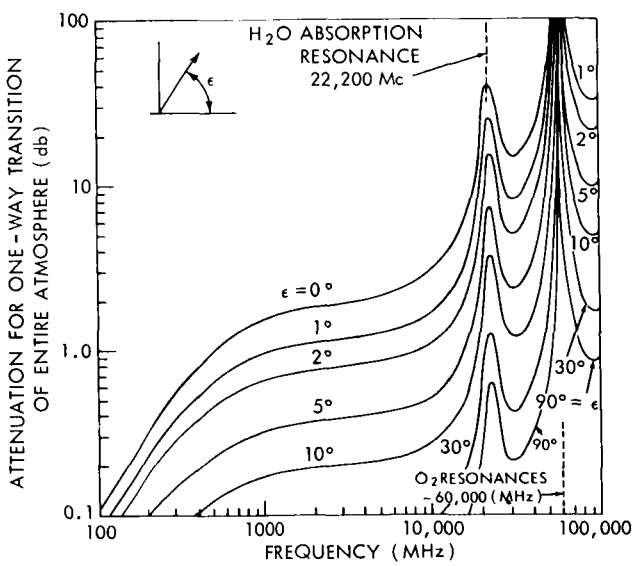

Figure 3(a)—One-way attenuation through the standard summer atmosphere due to oxygen and water vapor.

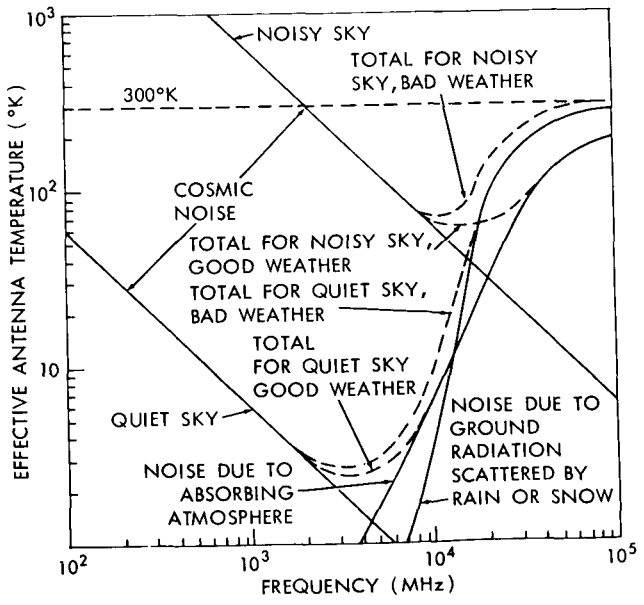

Figure 3(b)—Effective antenna temperature due to galactic noise and atmospheric absorption.

frequencies (some off-the-shelf and some still in the laboratory stage; see References 2 and 12), systems capabilities were also computed at these frequencies and are tabulated in Tables 2 and 3. The values used for the receiver noise temperatures were for the best available parametric amplifiers at 16 GHz and 34 GHz, while at 94 GHz the computations for the system capability were done for each of the best available crystal mixer, parametric amplifier, and maser (Reference 2).

Table 2

Analysis of Millimeter (16 GHz, 34 GHz) Transmission From Mars Space Vehicle to Earth-Based Station.

Parameter	Values	
	Freq = 16 GHz[4]	Freq = 34 GHz[4]
Wavelength	18.75 mm (0.06152 ft)	8.82 mm (0.02893 ft)
Range	1.852×10^8 km (10^8 n. mi.)	1.852×10^8 km (10^8 n. mi.)
Transmitter power, P_T	200 w[1] 23.0 dbw	200 w[1] 23.0 dbw
S/V antenna gain, G_T	4.85 m (15 ft) 55.0 db	4.85 m (15 ft) 61.7 db
Transmitter line loss, $1/L_T$	~-1.5 db	~-3.0 db
Free space path loss, $\lambda^2/(4\pi R)^2$	-281.8 db	-288.4 db
Receiver line loss,[5] $1/L_R$	~-0.5 db	~-1.0 db
Ground antenna gain, G_R	9.16 m (30 ft) 61.2 db	9.16 m (30 ft) 67.8 db
Receiver power, P_R	-144.6 dbw	-139.9 dbw
CNR = P_R/KTB	10.0 db	10.0 db
Allowable noise power	-154.6 dbw	-149.9 dbw
Effective system noise temperature: Receiver noise	438°K[2]	290°K[2]
Sky noise	14°K[3]	51°K[3]
Line noise	32°K	43°K
	-201.8 dbw/Hz	-202.2 dbw/Hz
Noise bandwidth	52.5 kHz 47.2 db Hz	170 kHz 52.3 db Hz
Maximum transmission rate	5.25×10^4 bits/sec.	1.70×10^5 bits/sec.

NOTES: (1) Assumed value based on 200w, cw, TWT at 94 GHz developed by Hughes Aircraft Co. (see Reference 2).
(2) Receiver noise for best available parametric amplifiers (see Reference 2).
(3) Sky noise, includes atmospheric absorption, good weather, quiet sky (Reference 9).
(4) Best available parametric amplifiers (see Reference 2).
(5) Assumes receiver first stage is mounted near antenna input to minimize receiver line loss.

Table 3

Analysis of Millimeter Wave (94 GHz) Transmission From a Mars Space Vehicle to Earth-Based Station.

Parameter	Values		
	Crystal mixer[1]	Paramp[1]	Maser[1]
Frequency	94 GHz	94 GHz	94 GHz
Wavelength	3.2 mm (0.01048 ft)	3.2 mm (0.01048 ft)	3.2 mm (0.01048 ft)
Range	1.852×10^8 (10^8 n. mi.)	1.852×10^8 (10^8 n. mi.)	1.852×10^8 (10^8 n. mi.)
Transmitter power, P_T	200 w 23.0 dbw	200 w 23.0 dbw	200 w 23.0 dbw
S/V antenna gain, G_T	4.58 m (15 ft) 70.0 db	4.58 m (15 ft) 70.0 db	4.58 m (15 ft) 70.0 db
Transmitter line loss, $1/L_T$	-4.0 db	-4.0 db	-4.0 db
Free space path loss, $\lambda^2/(4\pi R)^2$	-297.2 db	-297.2 db	-297.2 db
Receiver line loss,[4] $1/L_R$	-1.5 db	-1.5 db	-1.5 db
Ground antenna gain, G_R	4.58 m (15 ft) 70.0 db	4.58 m (15 ft) 70.0 db	4.58 m (15 ft) 70.0 db
Received power, P_R	-139.7 db	-139.7 db	-139.7 db
CNR = P_R/KTB	10.0 db	10.0 db	10.0 db
Allowable noise power	-149.7 dbw	-149.7 dbw	-149.7 dbw
Effective system noise temperature: Receiver noise[1]	5500°K[1]	870°K[1]	200°K[1]
Sky noise[2],[3]	212°K[2]	212°K[2]	212°K[2]
Line noise	85°K[3]	85°K[3]	85°K[3]
	-191.0 dbw/Hz	-198.0 dbw/Hz	-201.6 dbw/Hz
Noise bandwidth	13.5 kHz 41.3 db Hz	67.5 kHz 48.3 db Hz	15.5 kHz 51.9 db Hz
Maximum transmission rate	1.35×10^4 bits/sec	6.75×10^4 bits/sec	1.55×10^5 bits/sec

NOTES: (1) Best available (see Reference 2).
(2) Grimm, H. H., (Reference 9).
(3) Blake, L. V., (Reference 13).
(4) Assumes receiver first stage mounted near antenna input to minimize receiver line loss.

Optical Systems

In the case of optical systems where $hf >> kT$, the noise power density ψ for ideal detectors is given by

$$\psi \approx \begin{cases} hf/2 \text{ homodyne detection} \\ hf \text{ heterodyne detection} \\ 2hf \text{ non-coherent detection} \end{cases}$$

(see Reference 5). In practice, however, the detectors are not ideal.

For carrier signals in the visible and near infrared spectrum (i.e., about 0.4 μ to 1.1 μ), photoemissive devices, such as photomultiplier tubes, are suitable detectors. The response times of ordinary photomultipliers are between 1 and 3 nanoseconds, enabling them to detect modulation frequency in the order of 300 MHz. Although the performance of commercial photomultipliers begins to be degraded between a 50 MHz and 150 MHz modulation frequency, beat notes of up to 300 MHz in modulation frequency have been detected with an ordinary 7102 multiplier phototube (Reference 14). However, such devices emit a current even in the absence of illumination. This current is called a dark current and is a source of noise. The resulting noise equivalent power (NEP) in a one-cycle bandwidth for some typical photoemissive type tubes in the red visible region varies between 2×10^{-12} watt-sec$^{-1/2}$ and 10^{-17} watt-sec$^{-1/2}$ (see References 10 and 14), where the NEP is equal to the input signal which produces the same output voltage as is present in one-cycle bandwidth because of noise alone.

For carrier signals of wavelength greater than about 1.1 μ, where photoemissive devices are no longer operative, the p-n or p-I-n junction devices used in the photovoltaic mode might be used. They have response times of about 1 microsecond beyond approximately 1.0 μ, and nanosecond response times have been reported (see Reference 14), particularly in the visible and near-infrared spectrum. Their disadvantages are their capacity, which restricts the bandwidth over which they can be operated, and their sensitive area, which must be kept small to keep the capacitance small and response times fast. The most important source of noise in a photovoltaic detector is shot noise caused by the particle nature of the current. There is also thermal noise in the various resistive elements in the diode circuit. However, the shot noise due to the quantum effects, namely the quantum nature of electric charge and photons, can be made to predominate over the thermal noise by cooling the detector.

In the case of photoemissive type detectors, it is possible to achieve a condition where shot noise is dominant by using heterodyne operation (References 5 and 14). It has been shown (Reference 5) that both the shot noise power and signal power increase in the same proportion as the local oscillator power, making it possible for the shot noise power to overshadow the dark current noise without degrading the signal-to-noise ratio.

On the other hand, heterodyne operation has some disadvantages. First, there is the requirement for close alignment of the received signal beam with the local oscillator beam, because constructive interference between the two beams can occur only if they are aligned within an angle $\Delta\theta \leq \lambda d$, where λ is the wavelength of the received beam and d is the diameter of the collecting optics (Reference 14). Other disadvantages include the problems of coping with the local oscillator

instabilities and relatively large Doppler shifts because of the relative motion of transmitter and receiver. For instance, the one-way Doppler shift is

$$\Delta f_{Doppler} \approx \frac{\dot{r}}{\lambda} , \tag{11}$$

where $\dot{r}$ is the relative radial speed of the source and observer, or, in terms of ground tracking stati terminology, $\dot{r}$ is the range rate. In the case of a 200 day trajectory to Mars, launched December 26, 1971, after 12 hours out, the $\dot{r}$ varies from about 3 km/sec (approximately 10,000 fps) to about 16.4 km/sec (approximately 54,000 fps). From this, the resulting Doppler shift is tabulated (Table 4) for two of the more promising laser sources.

In addition to the shot noise, dark current noise, and thermal noise, there is also the background noise (i.e., all other noise entering the detector with the signal including the noise due to signal fluctuations).

Table 4

Doppler Shift for Argon II and CO_2 Lasers.

Type of laser source	Wavelength, λ (microns)	Doppler (Hz)	
		12 hrs. after injection	200 days after injection
Argon II	0.5	6×10^9	32.8×10^9
CO_2	10.6	2.8×10^8	15.5×10^8

The problems of optical background noise have been discussed, documented, and summarized in Reference 10, which in turn utilizes a large number of references. The optical background noise includes cosmic background (see Figure 4), solar radiation background (see Figure 5), lunar and planetary radiation (see Figure 6), and (in the case of a spacecraft "looking" at the

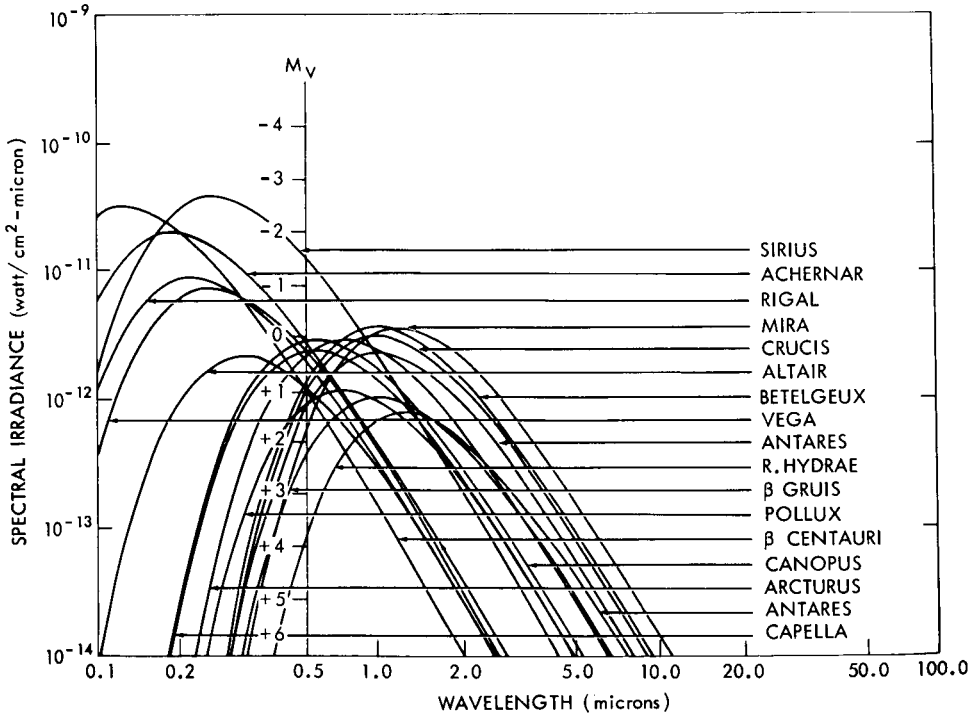

Figure 4—Spectral irradiance of brightest stars outside the terrestrial atmosphere.

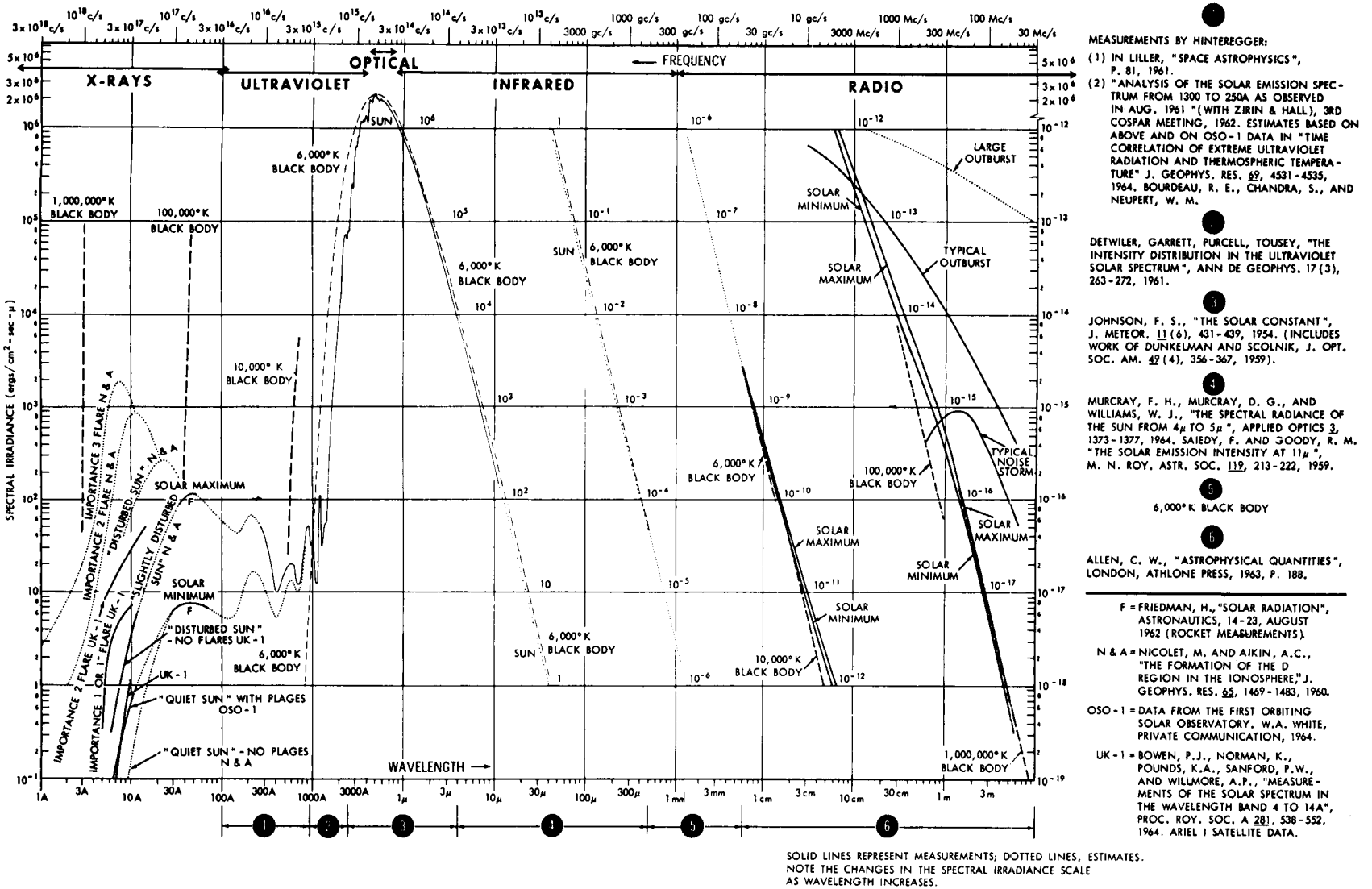

SOLID LINES REPRESENT MEASUREMENTS; DOTTED LINES, ESTIMATES.
NOTE THE CHANGES IN THE SPECTRAL IRRADIANCE SCALE AS WAVELENGTH INCREASES.

MEASUREMENTS BY HINTEREGGER:
(1) IN LILLER, "SPACE ASTROPHYSICS", P. 81, 1961.
(2) "ANALYSIS OF THE SOLAR EMISSION SPECTRUM FROM 1300 TO 250A AS OBSERVED IN AUG. 1961 "(WITH ZIRIN & HALL), 3RD COSPAR MEETING, 1962. ESTIMATES BASED ON ABOVE AND ON OSO-1 DATA IN "TIME CORRELATION OF EXTREME ULTRAVIOLET RADIATION AND THERMOSPHERIC TEMPERATURE" J. GEOPHYS. RES. 69, 4531-4535, 1964. BOURDEAU, R. E., CHANDRA, S., AND NEUPERT, W. M.

2 DETWILER, GARRETT, PURCELL, TOUSEY, "THE INTENSITY DISTRIBUTION IN THE ULTRAVIOLET SOLAR SPECTRUM", ANN DE GEOPHYS. 17(3), 263-272, 1961.

3 JOHNSON, F. S., "THE SOLAR CONSTANT", J. METEOR. 11(6), 431-439, 1954. (INCLUDES WORK OF DUNKELMAN AND SCOLNIK, J. OPT. SOC. AM. 49(4), 356-367, 1959).

4 MURCRAY, F. H., MURCRAY, D. G., AND WILLIAMS, W. J., "THE SPECTRAL RADIANCE OF THE SUN FROM 4μ TO 5μ", APPLIED OPTICS 3, 1373-1377, 1964. SAIEDY, F. AND GOODY, R. M. "THE SOLAR EMISSION INTENSITY AT 11μ", M. N. ROY. ASTR. SOC. 119, 213-222, 1959.

5 6,000° K BLACK BODY

6 ALLEN, C. W., "ASTROPHYSICAL QUANTITIES", LONDON, ATHLONE PRESS, 1963, P. 188.

F = FRIEDMAN, H., "SOLAR RADIATION", ASTRONAUTICS, 14-23, AUGUST 1962 (ROCKET MEASUREMENTS).

N & A = NICOLET, M. AND AIKIN, A.C., "THE FORMATION OF THE D REGION IN THE IONOSPHERE," J. GEOPHYS. RES. 65, 1469-1483, 1960.

OSO-1 = DATA FROM THE FIRST ORBITING SOLAR OBSERVATORY. W.A. WHITE, PRIVATE COMMUNICATION, 1964.

UK-1 = BOWEN, P.J., NORMAN, K., POUNDS, K.A., SANFORD, P.W., AND WILLMORE, A.P., "MEASUREMENTS OF THE SOLAR SPECTRUM IN THE WAVELENGTH BAND 4 TO 14A", PROC. ROY. SOC. A 281, 538-552, 1964. ARIEL 1 SATELLITE DATA.

Figure 5—The solar spectrum.

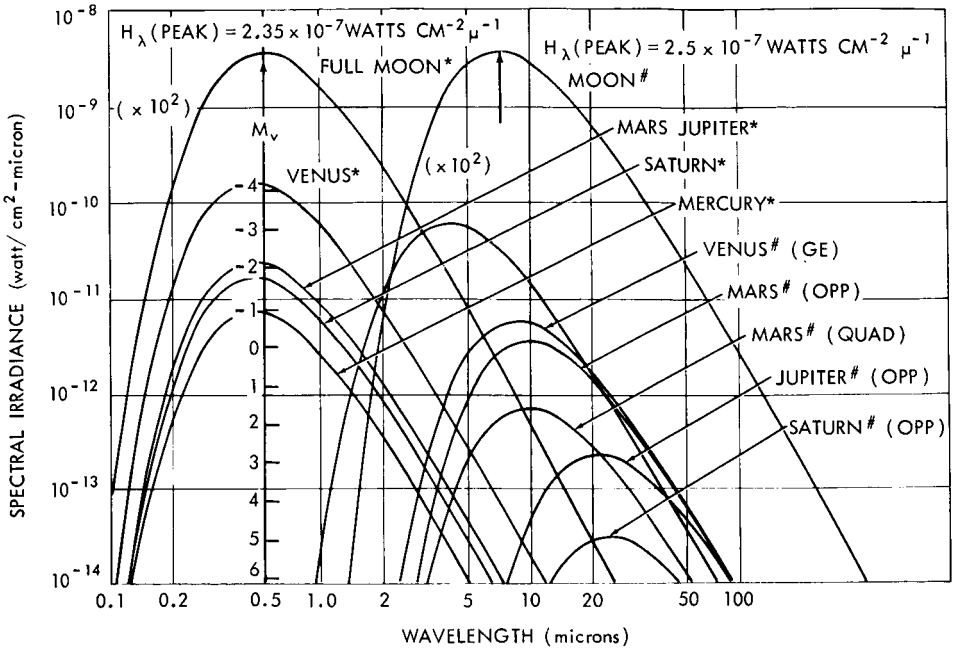

* - Calculated irradiance from planets, at brightest, due to sun reflectance only.

\# - Calculated irradiance from planets, due to self-emission only.

GE - Inferior planet at greatest elongation.

OPP - Superior planet at opposition.

QUAD - Superior planet at quadrature.

Figure 6—Calculated planetary and lunar spectral irradiance outside the terrestrial atmosphere.

earth) reflected solar and total earth radiation (see Figure 7). This latter figure does not include the fine spectra which could be an important factor in the selection of the optimum frequency for a ground beacon for acquisition and tracking of the earth terminal by the spacecraft.

Shown in Figures 8 and 9 is the atmosphere transmission at sea level for various elevation angles (or varying optical air masses) over the wavelength regions 0.3 μ to 1.3 μ and 1.2 μ to 5.0 μ, respectively.

An electromagnetic wave propagating through an ionized medium in the presence of a magnetic field undergoes a rotation of its plane of polarization. This is called Faraday rotation. In the propagation path between an earth terminal and a space vehicle, the ionized medium is the earth ionosphere, and the magnetic field is that of the earth. Because of the inverse-square relationship between frequency and Faraday rotation, the rotation could be a fraction of a radian at L-Band (Reference 15), and about 1 arc minute at light frequencies (Reference 16).

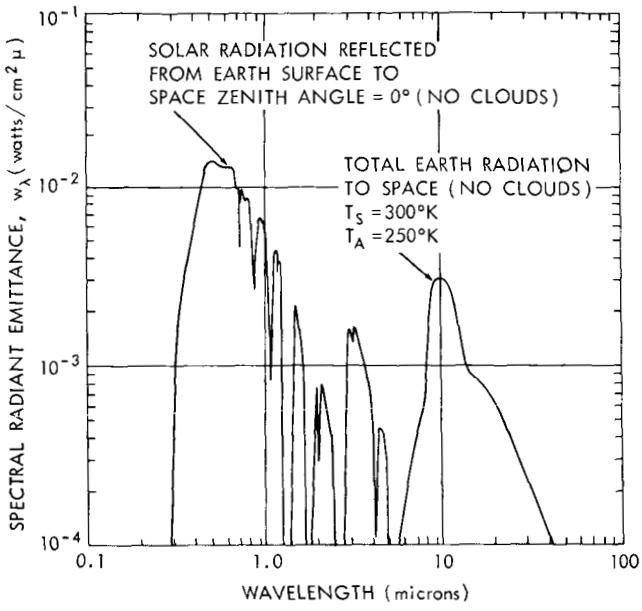

Figure 7—Solar and terrestrial radiation. Reflected solar and total earth radiation to space values should be divided by π to obtain the radiance for each case. T_S is the surface temperature and T_A is the effective radiating air temperature.

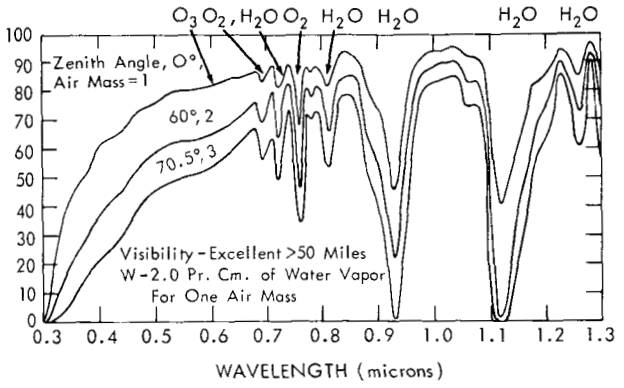

Figure 8—Transmission of the atmosphere at sea level for varying optical air masses. Atmospheric transmission, 0.3 to 1.3 microns.

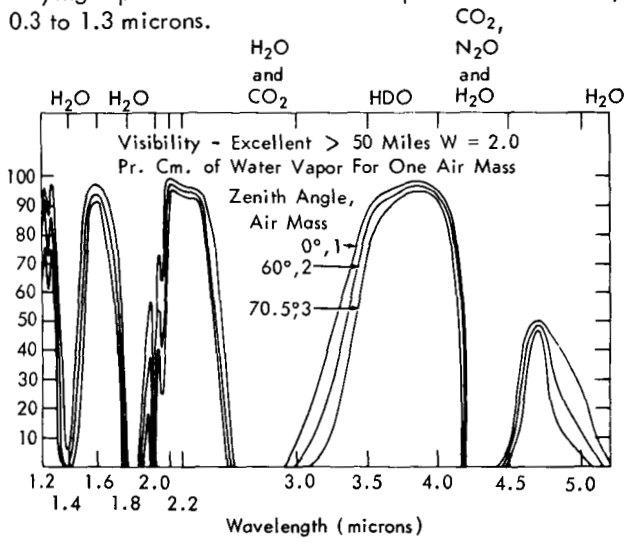

Figure 9—Transmission of the atmosphere at sea level for varying optical air masses. Atmospheric transmission, 1.2 to 5.0 microns. Gases responsible for valleys are indicated.

In recent years, the sun's magnetic field has been inferred from the polarization of sun spots. The polarization does not change with slanting look angles (Reference 16). In addition, measured polarization in the light from Crab Nebula and other nebulae tends to confirm physical theory which says that the atmosphere can have no more than small effects on the plane and degree of polarization of light. According to theory (Reference 15, p. 605), the one-way rotation of the plane of polarization may be written as

$$\Omega(\text{rad}) = \frac{2.35 \times 10^4}{f^2} \int_{h_1}^{h_2} NH \cos\theta \sec\chi \, dh \quad , \tag{12}$$

where,

f = frequency of electromagnetic radiation (Hz),

N = number of electrons per cubic centimeter,

H = strength of geomagnetic field (emu in gauss),

θ = angle between the direction of propagation and magnetic field,

χ = angle between direction of propagation and zenith at point where electromagnetic ray passes through the ionosphere,

and

dh = element of height in cm along line of sight between transmitter and receiver antennae.

The factors N, H, and θ are included under the integral sign because of their altitude dependence.

After a careful consideration of the foregoing factors and information capacity, it may be concluded (see also Reference 14) that:

1. The choice of a laser source in the atmosphere windows of the infrared spectrum, namely at approximately 3.5μ and 10.6μ, seems highly desirable particularly if suitable detectors can be found, since the information capacity increases with wavelength (see Figure 9 of Reference 14).

2. Existing lasers limit practical consideration to wavelengths $\leq$10.6μ, the wavelength of the CO_2 laser.

3. Antenna sizes and weights favor higher frequency operation to the point where the beam becomes so narrow that the problems of pointing and tracking and atmosphere image motion limit the advantages to be gained.

4. Using a ground-based terminal instead of a spaceborne relay favors noncoherent operation because of atmospheric effects and the possible use of larger apertures. However, heterodyne operation, if possible, would permit narrowband (IF) filtering, which would be valuable for decreasing the background noise.

5. Incoherent analogue modulation techniques do not compete with the more efficient time quantized forms of modulation.

6. PCM and PPM are the most efficient of the time-quantized forms of modulation.

7. For a high background noise environment, in the absence of signal noise, PCM is superior to PPM.

8. The three main forms of incoherent PCM modulation (namely PCM/AM, PCM/FSK, and PCM/PL) exhibit nearly the same communication system efficiency.

9. PCM/FSK and PCM/PL have the advantage over PCM/AM, since with a laser of peak power limitation, PCM/AM will be restricted to an operation at one-half the average power transmission of PCM/FSK and PCM/PL.

10. The Faraday effect causes a rotation of the plane of polarization of about 1 arc minute for light (Reference 16), which is not believed to be overly detrimental to the PCM/PL mode of operation

It is interesting to note that a PCM/PL (pulse code, polarization modulation) high data rate (approximately 30 Mbps) Argon II laser communication system with about 2 watts to 4 watts cw power

Table 5

CW Laser Oscillators (See Reference 10).

Active material	Wavelength (μ)	Output Power	Dimensions of active material	Comments	References in Reference 10
1. He-Ne	0.6118 0.6328 1.084 1.152	5 mw 50 mw 5 mw 20 mw	6 mm × 1.8 m	Single mode, commercially available	1
2. He-Ne	0.6328	900 mw	10 mm × 5.5 m	Research devices	2
3. He-Ne	0.6328	100 mw	5 mm × 1.2 m		
4. Xe	3.5 9.0	0.1 mw 0.5 mw	2.6 mm × 50 cm	Research device	3
5. Ar^+	0.4579(0.05) 0.4765(0.1) 0.4880(25) 0.4965(0.1) 0.5107(0.1) 0.5145(0.4)	10 w	6 mm × 60 cm	Research devices, 0.1 - 0.2% efficiency	4
6. Ar^+	(as in 5)	16 w	4 mm × 2.6 m		5
7. Ar^+	0.4880	1 w	3 mm × 45 cm	Airborne development device	6
8. CO_2	10.57(0.75) 10.59(0.25)	16 w	25 mm × 2.0 m	4.0% efficiency, single mode for each line	7
	10.59	135 w		15% efficiency	8
9. Cr^{+3}	0.6943	70 mw	2 mm × 2.54 cm	Water cooled	9
10. Nd^{+3} ($CaWO_4$)	1.06	1 w	3 mm × 3.5 cm	Methyl alcohol cooling (approximately 300°K)	10
11. Nd^{+++} (YAG)	1.06	1.5 w	2.5 mm × 3.0 cm		11
12. Nd^{+++} (YAG)	1.06	0.5 w	---	Water cooled, commercially available, portable	12
13. Dy^{+2} (CaF_2)	2.36	0.75 w	4.8 mm × 2.54 cm	Liquid neon (27°K) bath	13
14. GaAs	0.84	12 w	0.5 mm × 0.4 cm (diode dimensions)	Liquid He (4°K) bath, 23% efficiency	12

output is presently under development for the NASA Manned Spacecraft Center, Houston, Texas (Contract NAS9-4266). The receiver utilizes the noncoherent detection mode. In essence, depending on the polarization, the received signal will be separated by a prism (such as a Nicol prism, for example; see Reference 12, p. 499) and passed onto one of the two photocathode type detectors for noncoherent detection; i.e., they act essentially as photon counters.

For the ground terminal receiver, it has been proposed (see Reference 17) that a 30 meter spherical antenna be built as an optical analog of the 1000 foot Arecibo radio astronomy antenna. Although it is not probable that such an antenna will be ready for the missions to take place in the 1970's, it is included in the analysis. (Note: It was also included in the analyses of Reference 1).

Shown in Table 5 are some characteristics for several gas lasers. Based on the transmissivity of the atmosphere and the best gas laser sources (Table 5), some laser system communication capabilities were computed and tabulated in Table 6 for the case of communications from a spacecraft at Mars distances to an earth-based terminal utilizing the noncoherent detection mode.

Table 6

Mars Vehicle to Earth-Based Station Laser Transmission Analysis.

Parameter	Values			
	Ionized argon gas type laser		CO_2 type laser[8]	
Wavelength	0.5 μ		10.6 μ	
Range, R	1.852×10^8 km (10^8 n. mi.)		1.852×10^8 km (10^8 n. mi.)	
Transmitter power	4.0 w	6.0 dbw	130.0 w	21.1 dbw
DSV antenna gain[1]	12.7 cm	115.3 db	1 m	106.7 db
DSV transmission loss[2]	τ = 0.85	-0.7 db	$\tau \cong 0.7$	-1.4 db
Spreading loss	$1/4\pi R^2$	-236.7 db/m^2	$1/4\pi R^2$	-236.7 db/m^2
Minimum atmosphere loss[3,7]	0.40	-4.0 db	0.40	-4.0 db
Receiver aperture area[4]	78.5 m^2	18.9 dbm^2	78.5 m^2	29.3 dbm^2
Receiver loss[5]	0.27	-5.7 db	0.27	-5.7 db
Received power		-106.4 dbw		-100.6 dbw
CNR[6]		10.0 db		10.0 db
Detector quantum efficiency, η	0.20	-7.0 db	0.20	-7.0 db
Allowable noise power		-123.4 dbw		-117.6 dbw
hf	3.97×10^{-19}	-184.1 dbw/Hz	1.88×10^{-20}	-197.3 dbw/Hz
Noise bandwidth (2 B_0)	1.15 MHz	60.7 db Hz	93 MHz	79.7 db Hz
Maximum transmission rate	1.15×10^6 bits/sec		9.3×10^7 bits/sec	

NOTES: (1) For defraction limited beamwidth of 1 arc second at $\lambda = 0.5\mu$ and 2.67 arc seconds at $\lambda = 10.6\mu$.
(2) Beam deflector $\tau_1 = 0.85$; modulator $\tau_2 = 0.85$.
(3) Rain loss 30 db; fog and snow loss 80 db (Laser Letter July 1964, p. 3; see Reference 1 also).
(4) Assuming 30-meter spherical antenna, effective diameter is 10 meters.
(5) 10Å filter, $\tau_1 = 0.35$; antenna, $\tau_2 = 0.90$; beam deflector, $\tau_3 = 0.85$.
(6) CNR = $\eta P_s / 2hf B_0$, quantum noise limited; CNR = 10 db for $P_{e,s} \cong 2.3 \times 10^{-5}$ (bit error probe for PCM/PL mod.)
(7) Rain margins not included.
(8) Assumes quantum noise limited operation and that suitable detector(s) will become available.

In these computations, it was assumed that the minimum atmosphere loss is 0.4 or -4 db (see Reference 1) which seems to be a reasonable value when one notes the differences reported (Reference 14, Figure 11, which is repeated here as Figure 10) in the bandwidth capability for free space transmission versus ground-based terminal in daytime and nighttime operation. The two lasers

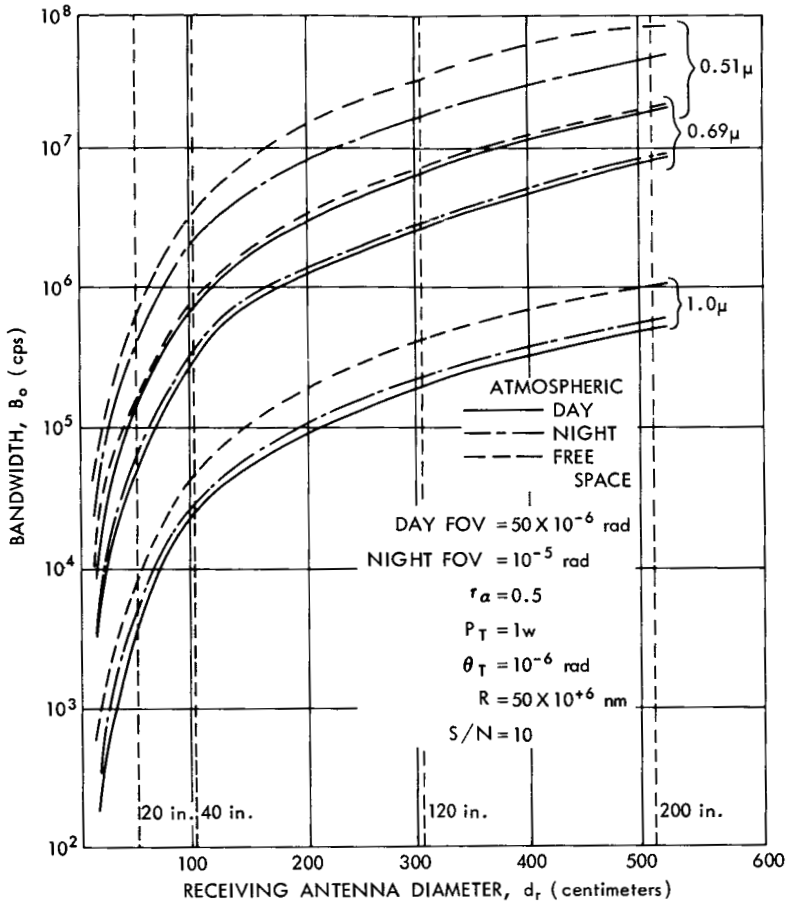

Figure 10—Some optical system communication capabilities at daytime, night, and in free space.

used were the 4 w argon II laser and the 130 w CO_2 laser compared in Table 6. The HeXe laser at 3.5 μ wavelength, which is at one of the atmosphere windows, was not treated because of its low power output and its relatively low efficiency. Table 7 lists some semiconductor materials which might be considered for the detector in a 10.6 μ laser system. Table 7 also gives their characteristic cutoff wavelength and maximum operating temperature. Their response times are not known, because there

Table 7

Characteristics of Semiconductor Materials for 10.6μ Detector (See Reference 10).

Detector material	$\lambda_{1/2}$, μ(1)	T_{max}, °K(2)
Ge:Au	~9	70
Ge:Hg	14	40
Ge:Cd	22	25
Ge:Cu	28	18
Hg_{1-x} Cd_x Te	12	77

(1) Wavelength at which detectivity decreases to 1/2 its peak value.
(2) Temperature at which detectivity decreases to $1/\sqrt{2}$ of its maximum value.

Table 8

Baker-Nunn Sites Showing Percentage of Time Lost Because of Clouds
(See Reference 10).

Station coordinates (long.)	Lat.	Year	Jan.	Feb.	Mar.	Apr.	May	June	July	Aug.	Sept.	Oct.	Nov.	Dec.
New Mexico 253°27'E	+32°25'	1962	36	25	27	15	5	12	49	32	48	19	26	22
		1963	34	27	21	29	30	13	48	57	28	16	27	17
South Africa 028°15'E	-25°58'	1962	42	29	31	26	4	6	1	5	8	29	53	37
		1963	50	23	27	28	15	21	20	2	7	30	55	49
Australia 136°46'E	-31°06'	1962	32	21	21	9	34	12	22	22	27	38	15	18
		1963	16	22	22	22	51	35	47	21	18	17	18	22
Spain 353°48'E	+36°28'	1962	52	32	81	43	33	15	21	15	34	47	40	43
		1963	72	49	39	39	35	32	4	19	22	19	60	45
Peru 288°30'E	-16°28'	1962	81	71	56	38	10	2	5	6	35	22	42	55
		1963	88	95	63	56	23	2	6	15	21	26	13	52
Iran 052°31'E	+29°38'	1962	28	44	33	54	10	1	18	16	03	nil	14	38
		1963	17	40	30	47	30	7	15	23	1	12	35	22
Curacao 291°10'E	+12°05'	1962	52	43	56	53	74	66	46	38	60	39	45	50
		1963	70	59	51	68	70	40	64	55	63	50	65	62
Florida 279°53'E	+27°01'	1962	55	40	62	55	36	61	41	55	52	45	55	43
		1963	57	58	47	28	50	42	44	29	49	32	49	43
Argentina 294°54'E	-31°57'	1962	53	52	38	72	51	27	39	32	22	29	35	43
		1963	*	35	40	27	39	33	36	32	57	46	46	30
Hawaii 203°45'E	+20°43'	1962	23	41	56	39	33	5	38	18	20	16	26	33
		1963	59	17	70	78	52	28	29	23	39	39	32	30

*No photography attempted for a 3-week period when the mirror was removed for realuminizing.

apparently had been no need to measure it heretofore. Table 8 gives some Baker-Nunn sites showing percentage of time lost because of cloud cover. More will be said about this in the next section. Table 9 summarizes the results of Tables 1 through 6.

Table 9

Comparison of Some Plausible Microwave, Millimeter Wave, and Optical Communication Systems at Mars Distances. ($R = 1.852 \times 10^8$ km (10^8 n. mi.), C/N = 10.0 db)

Parameter	Radio				Optical	
	S-Band	16 GHz	34 GHz	94 GHz	Argon II	CO_2[3]
f	2.3 GHz	16 GHz	34 GHz	94 GHz		
λ	13.05 cm (0.428 ft)	1.875 cm (0.06152 ft)	8.82 mm (0.02893 ft)	3.19 mm (0.01048 ft)	0.5 μ	10.6 μ
P_T	100 w	200 w	200 w	200 w	4 w	130 w
d_T	4.88 m (16 ft)	4.58 m (15 ft)	4.58 m (15 ft)	4.58 m (15 ft)	12.7 cm	1 m
G_T	38.8 db	55.0 db	61.7 db	70.0 db	115.3 db	106.7 db
$1/L_T$	~-1.0 db	~-1.5 db	~-3.0 db	~-4.0 db		
$1/L_R$		~-0.5 db	~-1.0 db	~-1.5 db		
d_R	64 m (210 ft)	9.16 m (30 ft)	9.16 m (30 ft)	4.58 m (15 ft)	10 m, eff.	10 m, eff.
G_R	60.0 db	61.2 db	67.8 db	70.0 db		
T[1]	50°K	484°K	384°K	497°K		
τ_R					0.27	0.27
τ_T					0.85	0.7
τ_a					0.4	0.4
η					0.2	0.2
$B_{max}^{(2)}$ bps	2.8×10^5	5.3×10^4	1.7×10^5	1.6×10^5	1.2×10^6	9.3×10^7

NOTES: (1) Effective system noise temperature; includes receiver noise, sky noise, and atmospheric attenuation.
(2) No margins included.
(3) Assumes quantum noise limited operation and that suitable detector(s) will become available.

Mission Analysis

Since the communication downlink at Mars distances is being considered in this report, let us now examine a Mars mission, at least in a preliminary fashion. Consider the case where a manned or unmanned spacecraft is on its way to Mars and is approximately 1.8×10^8 km away from the earth (see Figure 11). It is being tracked by the earth tracking network, and it is communicating with an earth ground station via a narrow laser beam. Ground stations strategically located to alleviate the cloud cover problem may be feasible (see Reference 18). For example, for a Baker-Nunn site located in New Mexico (253°27'E, 32°25'N) the observation time lost because of cloud cover varies between 5 percent and 49 percent depending on the time of year (see Table 13-2, Reference 10, given here as Table 8). The average time lost is approximately 25 percent. If one were to strategically locate a number of such sites, then the probability that at least one of these sites will not have cloud cover is

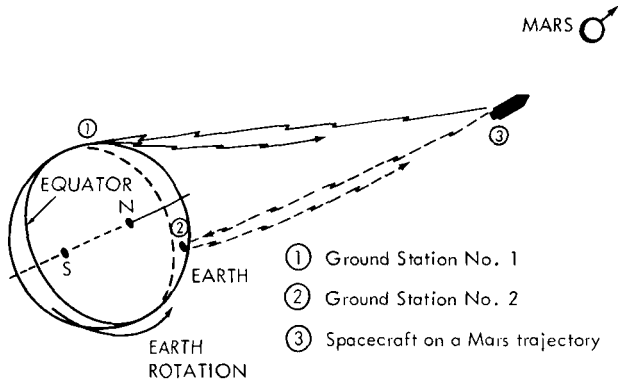

Figure 11—Top view of the ecliptic plane with a spacecraft on its way to Mars. An occultation is about to occur, and the spacecraft must switch over communication from ground station 1 to ground station 2.

$$P_{\text{no cloud}} = 1 - (P_{\text{cloud}})^n \quad , \tag{13}$$

where

n = number of sites,

P_{cloud} = probability of cloud cover at a site,

and

$P_{\text{no cloud}}$ = probability of no cloud cover at at least one of the sites.

Hence if $n = 4$ and $P_{\text{cloud}} = 0.25$ percent, then $P_{\text{no cloud}} = 0.996$.

It should be noted that in Equation 13, it is assumed that the probabilities of cloud cover at the various sites chosen are not correlated. Hence, in this sense the results obtained with Equation 13 may be optimistic. Furthermore, the results are pertinent only to occultations due to cloud cover. They do not consider occultations due to the earth rotation. For example, in the case shown in Figure 11, where an occultation is about to occur because of the earth rotation, the spacecraft must have the capability of switching over from one station to another whenever an occultation occurs whether it be due to cloud cover or planetary rotation, and so forth. The problem of acquisition and tracking associated with the use of very narrow laser beams has been studied to a limited extent (References 19 and 20); the results of these studies will be utilized in a further analysis of this problem by Hughes Aircraft Company on Contract NAS5-9637 (see References 2 and 10).

One possible acquisition and tracking mode which bears consideration is the technique used by Perkin-Elmer (Reference 16) on Stratoscope II. Experience with the balloon-borne Stratoscope II astronomical telescope, which utilizes stellar guidance techniques, indicates that the 3-ton gimbaled structure was stabilized at 1 or 2 arc seconds rms while its optical line of sight was directable by transfer lens action towards distant stars with pointing errors well within the 0.15-arc second diffraction limit of the instrument. Measurements indicate that line of sight errors in the order of 1/50 arc second or better may be expected with 9th magnitude or brighter stars for the 36-inch aperture instrument with an optical efficiency of about 30 percent from the aperture to the detectors (Reference 16). Consider the case wherein an earth laser beacon is utilized on the ground, and the Stratoscope II technique is used to acquire and lock onto (i.e., track) the ground beacon. Because of the propagation time delay (it takes a photon about 10 minutes to traverse 1.8×10^8 km in space) and the velocity aberration effects, the point ahead angle could be 300 times larger than the beam spread, assuming a very narrow laser beam of approximately 0.1 arc second for the downlink. Hence, the point ahead angle in this case must be controlled to within one part in 300 (see Appendix B for details). The vehicle may utilize the same telescope as both receiver and transmitter antennae and would acquire and track a light beacon on the earth. A course acquisition of the earth, which could appear as bright as about a -4th magnitude star at 1 A.U. (Reference 16), might be performed by the astronaut; the acquisition and tracking system might then perform the more vernier pointing by locking onto the earth beacon, which should be operating at a different laser frequency from the downlink. However, the earth is not always this bright, in which case direct detection of the earth beacon without resort to earth shine detection appears to be a requirement.

The magnitude of a star is its apparent brightness. The ancient Greeks devised the system still in use today, whereby the dimmest of stars ordinarily visible to the naked eye is +6, ranging upward to +1,0, and -1 for the very bright stars, -12 for the full moon as seen from the earth, and -27 for the sun. Each successive step on the scale represents a 2.5 multiplication of brightness.

Letting the vehicle share the same telescope for transmitter and receiver antennae has the advantages of smaller size and weight. However, it will be necessary to operate the earth beacon at a different laser frequency than the vehicle transmitting laser so that the vehicle can transmit and receive simultaneously without interference from scattered light or other detrimental effects.

Assume that the ground beacon uses an argon II, cw, gas laser at 0.5 μ wavelength and the vehicle uses the CO_2, cw, gas laser for the downlink. The problem is what amount of transmitted power is required of the ground beacon? We will now address ourselves to this problem, at least in a preliminary way. The position of the space vehicle may be determined to within a few hundred kilometers, based on Mariner IV success (see References 21 and 22). We will use an error of 400 km. The beamwidth of the ground beacon must be large enough to insure that the vehicle lies within the beamwidth, in which case

$$\theta_{\text{Beam gnd beacon}} = 2(3)\sqrt{\left(\frac{\sigma_{\text{S/C, pos}}}{R}\right)^2 + \left(\sigma_{\text{Beam point error}}\right)^2} \quad , \tag{14}$$

where

$\sigma_{S/C,\ pos}$ = standard deviation of spacecraft position error,

$\sigma_{Beam\ point\ error}$ = standard deviation of pointing the earth beacon,

and

R = slant range from ground beacon to spacecraft.

The factor of 2 is used because the errors can be plus or minus; the factor of 3 is used because the errors are one sigma, and to ensure a high probability (99.7 percent) that the spacecraft is in the beamwidth. Using $R = 1.852 \times 10^8$ km, $\sigma_{S/C,\ pos} \tilde{=} 400$ km, and σ (beam point error) = 2 arc seconds, which is within the capabilities of a high quality ground telescope pointing system; then $\theta_T = \theta$ (beam gnd. beacon) = 12 arc seconds = 58 μrad. We will use θ_T = 20 arc seconds to be conservative. It is assumed here that the atmosphere may be considered as part of the ground beacon optics so that θ_T is the width of the beam after it leaves the atmosphere. It is not known at this time just how much of the beam divergence is due to the atmosphere.

Figure 12 is a model block diagram which illustrates the operation of an optical, direct detection receiver (i.e., a noncoherent detection receiver). For such a receiver, it can be shown (Reference 10) that the signal-to-noise ratio at the detector output is given by

$$\frac{S}{N} = \frac{\eta P_s^2}{2B_0\, hf\, (P_s + P_b)} \quad , \tag{15}$$

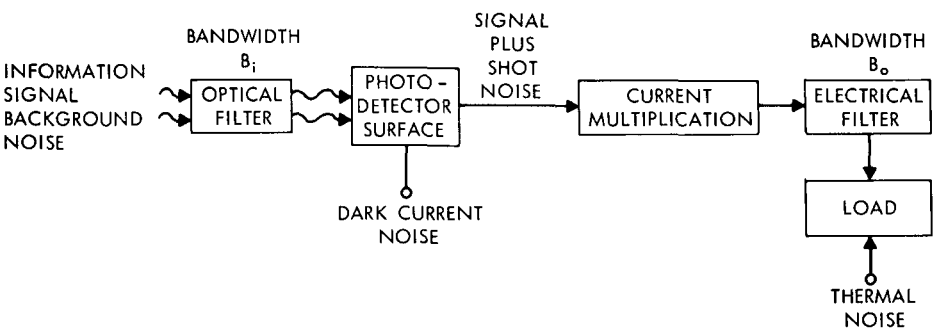

Figure 12—Direct or noncoherent detection model.

where it is assumed that (1) the photodetector is a photomultiplier with a gain of the order of 10^6 so that the shot noise and background noise are much larger than the thermal noise; (2) the detector is cooled so that its dark current may be neglected; and (3) the shot noise caused by the background is much larger than the background noise itself, which is usually the case (i.e., background shot noise >> direct background noise). When looking at an earth beacon, which is the case being considered here, then the received background power P_b due to the earth shine may be expected to be larger than the received signal power, in which case the signal-to-noise ratio at the

detector output is

$$\frac{S}{N} = \frac{\eta P_s^2}{2B_0\, hf\, P_b} \text{ for background limited operation} , \tag{16}$$

where B_0 is the effective bandwidth of the electrical filter following the detector; h is Planck's constant ($h = 6.624 \times 10^{-34}$ watt-sec^2); f is the laser transmitter frequency; η is the quantum efficiency of the detector (i.e., η is the number of photoelectrons emitted by the photocathode per incident photon); P_b is the received background noise power, which will be discussed subsequently; and P_s is the received signal power. We will use a value of 20 cps for B_0 (Mariner IV used a bandwidth of 1 bps for commands). It will be noted that when P_s is greater than the background power P_b, then

$$\frac{S}{N} = \frac{\eta P_s}{2B_0\, hf} \tag{17}$$

for signal quantum noise limited operation, which is the expression used earlier in computing the maximum information bandwidth in bits per second using a laser on the downlink from the spacecraft to the earth.

Let us now direct our attention to the uplink using an argon II laser as the ground beacon on the earth. The signal power received by the photodetector on the spacecraft is

$$P_s = \frac{P_T A_R \tau_a \tau_T \tau_R}{\frac{\pi}{4} R^2 \theta_T^2} , \tag{18}$$

where

P_T = power transmitted by the laser ground beacon, chosen to be an argon II laser for this example,

A_R = effective receiver aperture area,

τ_a = atmosphere transmissivity,

τ_T = transmitter transmissivity,

τ_R = receiver transmissivity,

R = distance between transmitter and receiver,

and

θ_T = whole beamwidth of the transmitted beam at the half-power points.

Assuming that $\tau_a = 0.4$; $\tau_R = 0.27$ (filter $\tau_1 = 0.35$, antenna $\tau_2 = 0.90$, beam deflector $\tau_3 = 0.85$); $\tau_T = 0.7$ (beam deflector $\tau_1 = 0.85$, modulator $\tau_2 = 0.85$) (see also Reference 1); $A_R = 0.785$ m^2;

$R = 1.852 \times 10^8$ km; $\theta_T = 10^{-4}$ rad as discussed above; then for the uplink

$$P_s = 1.74 \times 10^{-16} P_T \quad . \tag{19}$$

As will subsequently be seen for the case of the uplink, where the earth shine is a source for relatively large background noise, $P_b > P_s$, so that background limited operation results, and Equation 16 should be used in computing the received signal-to-noise ratio.

The background noise power received by the photodetector may be computed as follows. The radiant emittance of a Lambertian radiating source (the earth in this case) in watts per unit solid angle is given by

$$J = \frac{A'_{earth}}{\pi} \int_{\lambda_1}^{\lambda_2} W_\lambda \, d\lambda \quad , \tag{20}$$

where A'_{earth} is the area of the earth within the field of view of the spacecraft receiver optics, and where W_λ is the radiant emittance of the earth in watts per unit area per unit wavelength. Typical values of W_λ for the earth over the spectrum of interest are shown in Figure 7. The $\lambda_2 - \lambda_1$ is the bandwidth of the optical filter in the receiver, which for the uplink case being considered is on the spacecraft. Practical values for $\Delta\lambda = \lambda_2 - \lambda_1$ are from 1 to 10 Å, or 10^{-4} to $10^{-3}\mu$. Hence the background noise power P_b received at the photodetector is given by

$$P_b = J \tau_R \, d\Omega \quad , \tag{21}$$

where $d\Omega$ is the solid angle subtended by the receiver aperture and is

$$d\Omega = \frac{A_R}{R^2} \quad . \tag{22}$$

Substituting into Equation 21 for J and $d\Omega$ from Equations 20 and 22, then

$$P_b = \frac{A'_{earth} \, W_{\lambda_1 - \lambda_2} \, \Delta\lambda \, A_R \, \tau_R}{\pi R^2} \quad . \tag{23}$$

Let us now examine if the optical bandwidth $\Delta\lambda = 1$ Å is wide enough to handle the change in wavelength due to Doppler shifts, $\Delta\lambda_{Doppler}$, which is given by

$$\frac{\Delta\lambda_{Doppler}}{\lambda} = \frac{\Delta f_{Doppler}}{f} = \frac{\dot{r}}{c} \quad , \tag{24}$$

from which it is found that

$$\Delta\lambda_{Doppler} \doteq 0.5 \times 10^{-5}\,\mu \text{ to } 2.7 \times 10^{-5}\,\mu \ .$$

Hence, it appears likely that an optical filter as narrow as $10^{-4}\,\mu$ (or 1 Å) might be practical. In any event, a $10^{-4}\,\mu$ optical filter will be assumed for this example. From Figure 7, at $\lambda = 0.5\mu$, the $W_\lambda = 1.3 \times 10^2$ watts/$m^2 - \mu$. The received background power falling on the photodetector is, for the case considered,

$$P_b = 2.56 \times 10^{-26} A'_{earth}, \text{ watts} \ , \tag{25}$$

when A'_{earth} is in units of m^2. In the following paragraph, the A'_{earth} will be examined from an overall system point of view.

As pointed out earlier, the optical line of sight of the spacecraft receiver optics is directable towards distant stars to well within the 0.15 arc second diffraction limit of a 1 meter aperture instrument with an optical efficiency of about 30 percent from the aperture to the detectors (Reference 16). Hence, assume that the spacecraft receiver optics is "looking" at the bright earth, and its field of view is such that it only "sees" one-hundredth of the earth surface, i.e.,

$$A'_{earth} = \frac{A_{earth}}{100} = 1.277 \times 10^{12}\ m^2 \ . \tag{26}$$

Then the angular field of view θ_R' of the spacecraft receiver optics is obtained from

$$A'_{earth} = \frac{\pi}{4}\left(R\,\theta_R'\right)^2 \ ; \tag{27}$$

$$\therefore \theta_R' = 6.9 \times 10^{-6} \text{ rad} = 1.42 \text{ arc second} \ ,$$

which is an order of magnitude larger than the capability of directing the receiver telescope to well within 0.15 arc second. It should be noted that the angular field of view is not the diffraction limited beam angle. The field of view of the spacecraft receiver optics depends on the optical focal length f and the diameter of the field stop $d_{field\ stop}$ of the receiver optics; i.e.,

$$\theta_R' = \frac{d_{field\ stop}}{\text{focal length}} \ , \tag{28}$$

while the diffraction limited beam angle θ_R is related to the wavelength λ of the beam and diameter d_R of the receiver aperture, i.e.,

$$\theta_R = \frac{\lambda}{d_R} \ . \tag{29}$$

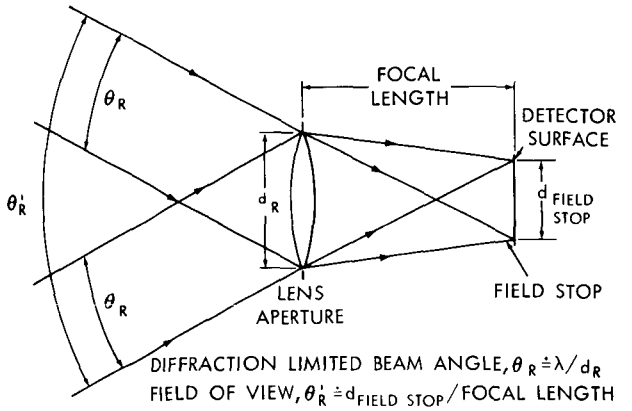

Figure 13—Illustration of beam divergence angle (θ_R) and angular field of view (θ_R').

The difference between the diffraction limited beam angle and the field of view is diagrammatically depicted in Figure 13.

The diameter d'_{earth} of the earth area A'_{earth} "seen" by the receiver optics, i.e., within the field of view, at Mars distances is

$$d'_{earth} = R\theta'_{earth} = 1280 \text{ km (690 nm)} , \quad (30)$$

which is one-tenth the diameter of the earth. Hence, in order to acquire the ground beacon, the spacecraft could scan a 10×10 raster with a total scan time (T_{scan}) of 100 seconds (1-2/3 min), which corresponds to a dwell time of 1 second per field of view.

During the scan mode, the probability of detecting the ground beacon (assuming that it is in the search field) is a function of both the signal-to-noise ratio and the $\log_{10}(T_{fa}/t_d)$, (see Figure 13-4 of Reference 23) where

$$T_{fa} = \frac{T_{scan}}{\eta_{fa}} = \text{mean time between false alarms} , \quad (31)$$

where

η_{fa} = number of false alarms for each complete scan of the search field (in this case the earth)

and

t_d = dwell time, i.e., the time that the instantaneous field of view rests on each point in the total field.

Hence

$$t_d = \frac{T_{scan}}{[A_{earth}/A'_{earth}]} = 1 \text{ second in this case} . \quad (32)$$

For $\eta_{fa} = 10^{-2}$, i.e., 1 false alarm per 100 complete scans of the search field, then

$$\log_{10}(T_{fa}/t_d) = \log_{10}\left(\frac{A_{earth}}{\eta_{fa} A'_{earth}}\right) = 2 - \log_{10}\eta_{fa} = 4 . \quad (33)$$

For a signal-to-noise power ratio of 10, which corresponds to a peak signal voltage-to-rms noise voltage ratio of 4.5, then from Figure 13-4 of Reference 23, the probability of detecting the ground beacon in one scan of the search field P_D is

$$P_D = 0.6 \ .$$

The cumulative probability P_C of detecting the ground beacon after j scans of the search field is

$$P_C = 1 - (1 - P_D)^j \ , \tag{34}$$

assuming that independent results are obtained on each scan (see Reference 24). Hence for $j = 3$, $P_C = 0.936$. That is, the cumulative probability of detecting the ground beacon in 3 complete scans (or 5 minutes of scan time at 100 seconds per scan) is 93.6 percent for a $S/N = 10$, which subsequently will be used to determine the required beacon transmitter power.

Using

$$A'_{earth} = \frac{A'_{earth}}{100} = 1.277 \times 10^{12} \, m^2 \ ,$$

the received background noise power at the detector, from Equation 24, is

$$P_b = 3.26 \times 10^{-14} \text{ watts} \ . \tag{35}$$

Solving for the required ground beacon transmitter power P_T as given by Equation 16,

$$P_T = 8.55 \sqrt{\frac{S}{N}} \text{ , watts} \ . \tag{36}$$

Hence, for a signal-to-noise ratio of 10, $P_T \doteq 27$ watts, which is beyond the present state-of-the-art technology for an argon II laser, but is not an overwhelming obstacle.

It is interesting to note that for this case of background noise limited operation, increasing the transmitted power by a factor of 2 increases the signal-to-noise ratio by a factor of 4 and would increase the probability of detection P_D discussed earlier, from 0.6 to 0.9999 per scan of the search field.

It should be noted that in planning a Mars mission, the launch date and flight time should be scheduled so that the earth-sun-Mars angle at the time of intercept is small enough (preferably approximately = 90 degrees) so that the background noise from the sun would be low; i.e., the sun would be far removed from the line of sight between the vehicle and earth. Shown in Figure 14 are

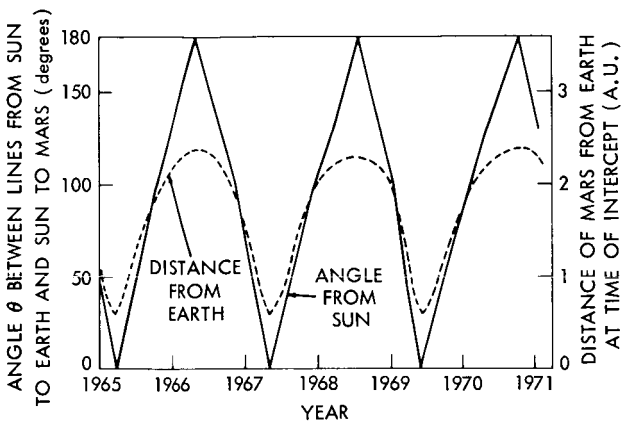

Figure 14—Angle θ and distance from earth to Mars at time of intercept.

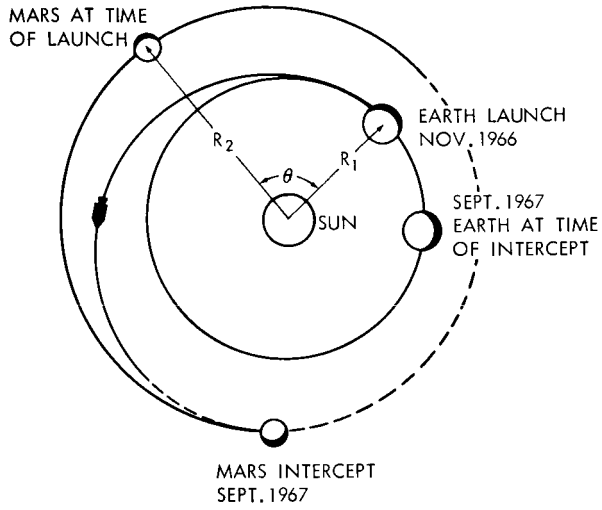

Figure 15—Possible Mars trajectory.

typical distances (R) of Mars from the earth at time of intercept and earth-sun-Mars angle at time of intercept (Reference 25). Shown in Figure 15 is a possible Mars trajectory, wherein the earth-sun-Mars angle is approximately 90 degrees, so that background noise from the sun would be small as discussed above. The launch date for this trajectory is November 1966, and the intercept date is September 1967. Furthermore, a patched conic Mars trajectory (Reference 26) was made to determine the time history of a flight trajectory to Mars during the year 1971. Table 10 gives the time history of this trajectory. The following are the symbol definitions used in Table 10; Figure 16 pictorially defines these symbols. Figure 17 is a plot of this trajectory. From the viewpoint of solar background noise, this latter trajectory appears to be somewhat better than the former trajectory.

Symbols used in Table 10 and Figure 16 are as follows:

RVS — Angle between the reference vector and the sun, read as Reference, Vehicle, Sun Angle;

RVE — Reference, Vehicle, Earth Angle;

RVT — Reference, Vehicle, Target Angle;

RFT — Radius from the Target body;

RFS — Radius from the Sun;

RFE — Radius from the Earth;

and

EVSA — Earth, Vehicle, Sun Angle.

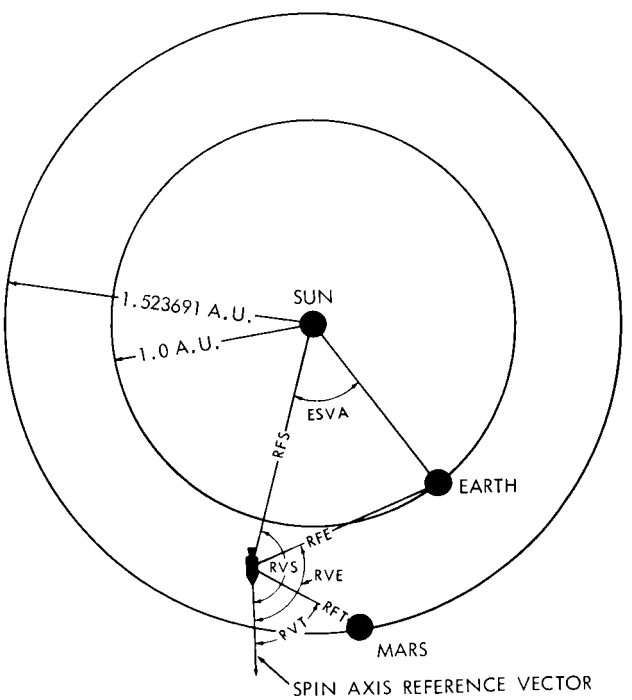

Figure 16—Earth-Mars trajectory geometry, pictorially defining some symbols used in computer printout.

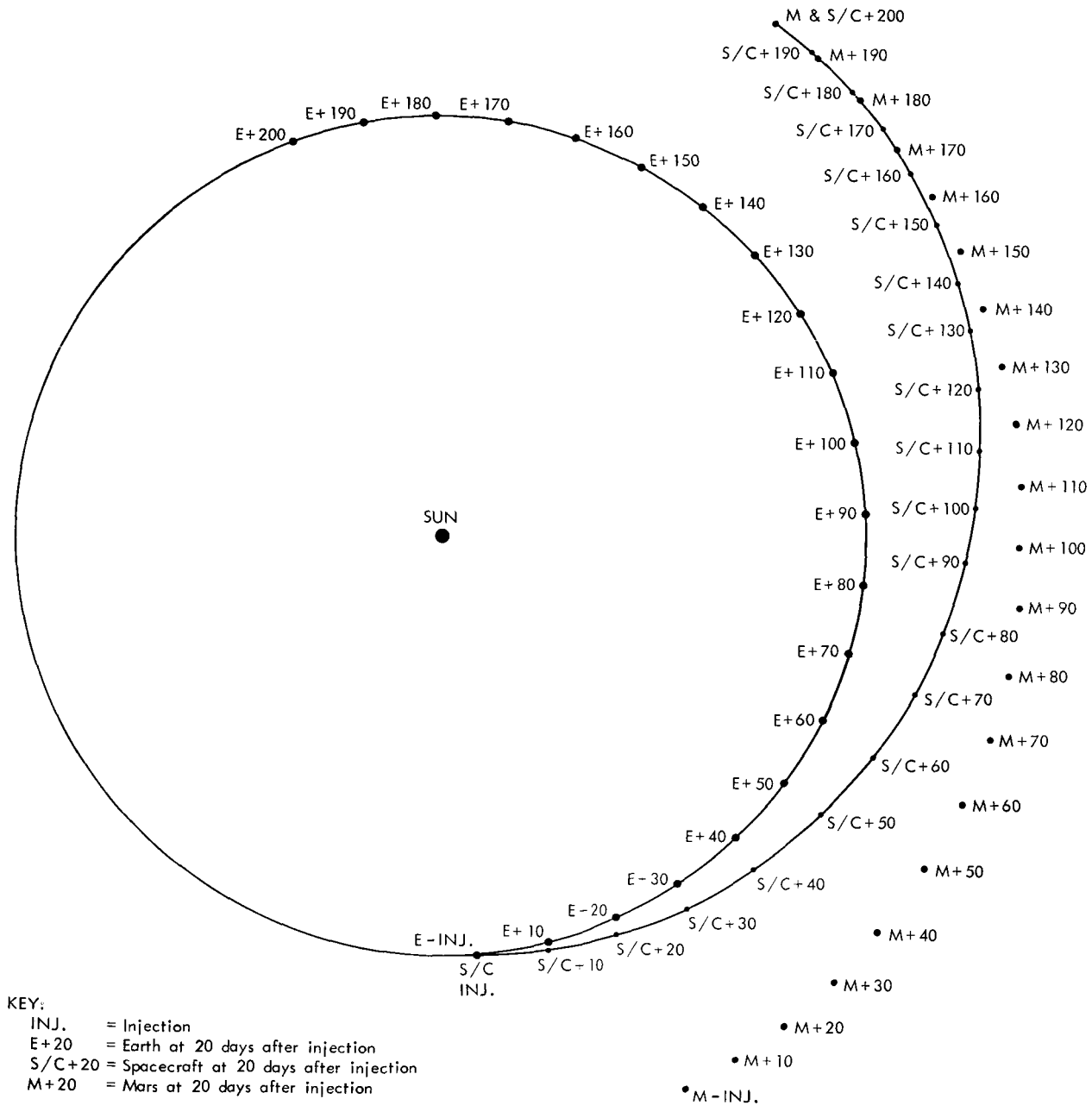

Figure 17—Earth-Mars trajectory.

SUMMARY

Given in Table 9 is a summary comparison of some plausible microwave, millimeter wave, and optical communication systems at Mars distances. It is believed that the systems considered are plausible in the sense that the values used for the various parameters are representative of state-of-the-art hardware, either off-the-shelf or now working in the laboratory, except in the cases of the optical ground receiver antenna (30-meter spherical) which has been proposed (see References 1

Table 10

Earth-Mars Trajectory Data.

(Injection: June 11, 1971 Julian date: 2441114.2530768
Mars intercept: Dec. 28, 1971 Julian date: 2441314.25307083)

D H M	V (km/sec)	γ (deg.)	$\dot{r}$ (km/sec)	$\dot{r}$ (fps)	RFS (km)	RFE (km)	RFT (km)	RVE (deg.)	RVS (deg.)	RVT (deg.)	ESVA (deg.)
0 0 19.5	11.43	0	0	0	151,910,000	6,560	89,559,090	90.0	174.98	57.24	0.0000057
0 12 19.5	3.65	83.76	3.6	11,800	152,200,000	188,980	88,893,130	126.4	174.88	57.39	0.055
1 0 19.5	3.386	86.26	3.3	10,850	152,120,000	339,360	88,272,720	123.56	174.74	57.55	0.104
5 0 0	3.154	89.26	3.1	10,200	152,830,000	1,440,290	83,508,450	120.62	172.34	58.68	0.437
10 0 0	3.157	89.47	3.1	10,200	153,880,000	2,802,310	77,769,030	120.51	167.97	59.94	0.793
20 0 0	3.264	87.10	3.2	10,500	156,470,000	5,565,430	67,092,870	121.59	158.46	61.88	1.281
30 0 0	3.514	84.51	3.5	11,500	159,630,000	8,472,660	57,583,510	123.29	148.99	62.94	1.415
40 0 0	4.027	82.59	4.0	13,100	163,270,000	11,685,300	49,313,550	125.398	139.85	63.04	1.141
50 0 0	4.803	83.47	4.8	15,800	167,260,000	15,456,000	42,301,130	127.38	131.08	62.14	0.4666
60 0 0	5.751	86.03	5.7	18,700	171,490,000	19,983,000	36,504,510	128.69	122.72	60.29	0.8095
70 0 0	6.899	88.76	6.8	22,400	175,870,000	25,429,000	31,818,830	129.15	114.76	57.69	2.394
80 0 0	8.164	85.21	8.1	26,700	180,300,000	31,923,000	28,079,890	128.62	107.19	54.61	4.429
90 0 0	9.492	80.72	9.3	30,600	184,710,000	39,483,000	25,070,110	127.12	99.98	51.42	6.873
100 0 0	10.93	76.23	10.6	35,000	189,020,000	48,118,000	22,596,590	124.82	93.10	48.44	9.707
110 0 0	12.39	71.72	11.8	38,800	193,190,000	57,797,000	20,421,790	121.81	86.52	45.90	12.899
120 0 0	13.88	67.57	12.8	42,100	197,160,000	68,426,000	18,386,490	118.22	80.22	43.90	16.42
130 0 0	15.42	63.54	13.6	44,700	200,898,000	79,940,000	16,369,220	114.18	74.15	42.45	20.24
140 0 0	16.94	59.59	14.5	47,600	204,360,000	92,220,000	14,294,380	109.76	68.31	41.49	24.33
150 0 0	18.46	55.90	15.3	50,300	207,530,000	105,150,000	12,124,180	105.02	62.65	40.94	28.66
160 0 0	20.01	52.29	15.9	52,300	210,380,000	118,600,000	9,848,820	100.04	57.15	40.68	33.20
170 0 0	21.52	48.73	16.0	52,500	212,899,000	132,440,000	7,477,420	94.85	51.80	40.62	37.93
180 0 0	23.01	45.36	16.4	54,000	215,060,000	146,510,000	5,030,370	89.48	46.57	40.63	42.80
190 0 0	24.50	45.03	16.3	53,600	216,870,000	160,680,000	2,533,420	83.96	41.44	40.54	47.81
200 0 0	24.74	39.69	15.7	51,700	218,290,000	174,810,000	12,831	78.31	36.40	56.06	52.90

and 17) as an optical analogue of the 1000-ft Aricebo radio astronomy antenna, and the present lack of suitable detectors in the infrared spectrum. From Table 9 and Figure 3, it may be concluded that, for spacecraft-to-ground communications, the S-Band appears to be the better place to operate in the radio spectrum, and the optical communication systems show considerable promise for supplying high data rates (theoretically up to approximately 10^8 bps) at Mars distances. However, considerable work remains to be done to make the optical system operational, particularly the development of flight-tested hardware, improving the lifetime expectancy of the laser tubes, solving the problem of acquisition and tracking associated with the very narrow laser beams, gaining a better understanding of the atmospheric effects on laser beams, and development of suitable detectors in the infrared spectrum.

Goddard Space Flight Center
National Aeronautics and Space Administration
Greenbelt, Maryland, October 31, 1966
125-21-02-17-51

REFERENCES

1. Gubin, S., Marsten, R. B., and Silverman, D., "Lasers Versus Microwaves in Space Communications," Astro-Electronics Division, Defense Electronic Products, Radio Corporation of America, Princeton, N. J. (Prepublication copy received Nov. 1965).
2. "Parametric Analysis of Microwave and Laser Systems for Communication and Tracking," by Hughes Aircraft Co. for NASA-GSFC, Contract NAS5-9637, Report No. P65-149, Nov. 30, 1965.
3. Chase, R. H., "NASA Space Optical Technology Program," presented at the Space Optical Technology Conference, Marshall Space Flight Center, Huntsville, Alabama, Nov. 2-4, 1965.
4. Van Atta, L. C., "Preparation for Communications and Research in Deep Space," presented at the 1966 Tuesday Evening Lecture Series entitled *Microwaves in Space* National Bureau of Standards, Washington, D. C., Jan. 11, 1966.
5. Oliver, B. M., "Thermal and Quantum Noise," *Proc. IEEE,* 436-454, May, 1965.
6. Rice, S. O., "Mathematical Analysis of Random Noise," *Bell Sys. Tech. J.* 22, p. 282, 1944; 25, p. 25, 1945.
7. Johnson, J. B., "Thermal Agitation of Electricity in Conductors," *Phys. Rev.* 32, p. 97, July 1928.
8. Nyquist, H., "Thermal Agitation of Electric Charge in Conductors," *Phys. Rev.* 32, p. 110, July 1928.

9. Grimm, H. G., "Fundamental Limitations of External Noise," *IRE Transactions on Instrumentation,* pp. 97-103, Dec. 1959.

10. "Reference Data for Advanced Space Communication and Tracking Systems," by Hughes Aircraft Company for NASA-GSFC Contract NAS5-9637, Report No. P 66-16, Feb. 6, 1966.

11. "New Hughes 9 KW-CW, C-Band TWT," *Missiles and Rockets,* 44-45, January 31, 1966.

12. Hoffman, L. A., Wintronb, H. J., and Garber, W. A., "Propagation Factors at 3.2 Millimeters," by Aerospace Corporation, Los Angeles, Calif. for Ballistic Systems and Space Systems Divisions, Air Force Systems Command, Los Angeles Air Force Station, Contract No. AF04 (695)-469, Report No. TDR-469 (5230-41)-6, October 1965.

13. Blake, L. V., "Tropospheric Absorption and Noise Temperature for a Standard Atmosphere," Summary of Paper for Presentation at the 1963 PT-GAP International Symposium, National Bureau of Standards, Boulder, Colorado, July 9-11, 1963.

14. Brinkman, K. L., and Pratt, W. K., "Design of a Laser Deep Space Communication System," Space Systems Division, Hughes Aircraft Company, El Segundo, Calif., prepublication copy, received Jan. 1966.

15. Skolnik, M. I., "Introduction to Radar Systems," New York: McGraw-Hill Book Company, 1962.

16. "Determination of Optical Technology Experiments for a Satellite," by Perkin-Elmer, Electro-Optical Division, Norwalk, Connecticut, for NASA-MSFC, Contract NAS8-11408, Engineering Report No. 7924, Feb. 1965.

17. Fusca, J. A., "Laser Communications," *S/A,* p. 57, May 1964.

18. "Deep Space Optical Communication Study," by Hughes Aircraft Co., Culver City, Calif., for NASA-MSC, Contract NAS9-879, 1st to 4th Interim Progress and Final Reports, 1963.

19. "Deep Space Laser Acquisition and Tracking Study," by Northrop Space Laboratories, Hawthorne, Calif., for NASA-MSC, Contract NAS9-2769, Report No. NSL64-270, Nov. 1964.

20. "Study of Laser Pointing Problems," by Kollsman Instrument Corp., Corporate Technology Center, Elmhurst, New York 11373, for NASA Hq. NAS W-929, 1964.

21. Clark, V. C., Jr., Roth, R. Y., Bollman, W. E., Hamilton, T. W., and Pfeiffer, C. G., "Earth-Mars Trajectories, 1964," Jet Propulsion Laboratory, Pasadena, Calif., Technical Memorandum No. 33-100, Vol. 1, March 1964.

22. "Interplanetary Navigation and Guidance Study," Vol. I-Summary, by Philco, WDL Division, Palo Alto, California, for Marshall Space Flight Center, Huntsville, Ala., Contract No. NAS8-11198, Report No. WDL-TR2629, Oct. 30, 1965.

23. Jamieson, J. A., McFee, R. H., Plass, G. N., Grube, R. H., and Richards, R. G., "Infrared Physics and Engineering," New York: McGraw-Hill Book Company, 1963.

24. Barton, D. K., "Radar System Analysis," Englewood Cliffs: Prentice-Hall, Inc., 1964.

25. Battin, R. H., "Astronautical Guidance," New York: McGraw-Hill Book Company, 1964.

26. "Users Manual for Quick-Look Mission Analysis Program" by Philco, WDL Div., for NASA-GSFC, Contract NAS5-3342, Report No. WDL-TR2218, Jan. 24, 1964.

27. Schwartz, M., "Information Transmission, Modulation, and Noise," New York: McGraw-Hill Book Company, 1959.

28. Barton, D. K., "Radar System Analysis," Englewood Cliffs: Prentice-Hall, Inc., 1964.

Appendix A

Noise Figure and Effective Noise Temperature

An ideal amplifier or detector is one which is noiseless, i.e., it introduces no noise to the noise already present at the input. A noise factor F (sometimes called a noise figure) is commonly used to describe the noisiness of a network.

The noisiness of a particular system or part thereof can be measured by comparing S/N at output and input. This measure of the noisiness of a system is called the noise figure F of the system and it is defined as

$$F = \frac{S_s/N_s}{S_0/N_0} \quad , \tag{A1}$$

with S_0/N_0 the signal-to-noise ratio in power at the output and S_s/N_s the signal-to-noise ratio in power at the input (source). An ideal network is thus one whose noise figure is unity (i.e., no additional noise introduced in the system). As F increases, the noisiness of the system increases (see also Reference 27). Noise figures are frequently measured or given in decibels since F is a ratio of power ratios, the conversion simply being $10 \log_{10} F$.

The concept of noise figure is particularly useful in the radio wave spectrum such as the microwave and millimeter wave, for instance. Radar receivers in the gc range using crystal converters frequently have noise figures ranging from 10 to 15 db; i.e., F ranging from 10 to 40. Most (or much) of the noise is developed in the system. A decrease of only 3 db in the noise figure of a typical system would reduce the power requirements of the radar transmitter by a factor of two. Hence, the question of decreasing system noise figures is of great importance.

The maximum power available at the output of a system, under matched conditions, is frequently called the available power. Thus, for a source represented by rms signal voltage e_s and output resistance R_s (sometimes referred to as the internal resistance of an equivalent signal source generator; see Figure A1), and under matched conditions (i.e., the load resistance is matched to R_s), the signal-to-noise ratio at the source is (see Reference 27, p. 231)

$$\frac{S_s}{N_s} = \frac{\text{available signal power}}{\text{available noise power}} \quad . \tag{A2}$$

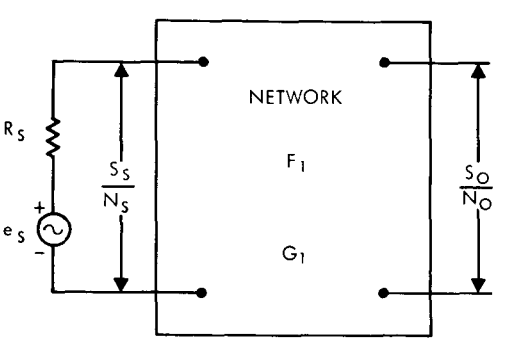

Figure A1—Linear network.

If G is the available power gain of a network and is defined as the ratio of available output signal power to available input signal power, i.e., $S_0 = GS_s$, then the noise figure can be written as

$$F = \frac{N_0}{GN_s} \quad . \tag{A3}$$

The equation $F = (N_0/GN_s)$ presents an alternative form for the equation of noise figure (aside from the definition in terms of S/N ratios) and is frequently given as the basic definition of F. Thus F may be defined as the ratio of actual noise power available from a network to that which would be available if the network were noiseless (Reference 27, p. 232).

Let us now examine how the noise figure can be related to an effective (or equivalent) system noise temperature, T. In the case of microwave and millimeter systems where $kT >> hf$, then the noise power density given by Equation 6 becomes

$$\psi \cong kT \tag{A4}$$

and

$$N = kTB \quad , \tag{A5}$$

with B being the effective bandwidth of the system.

Consider first a single linear network, and then a system of cascaded networks. Referring to Figure A1, the available noise power at the network output is

$$N_0 = G_1 N_s + N_1 \quad , \tag{A6}$$

where N_1 is the noise power contributed by the network at its output. Thus

$$F_1 = \frac{N_0}{G_1 N_s} = 1 + \frac{N_1}{G_1 N_s} \quad , \tag{A7}$$

or

$$(F_1 - 1)\, G_1 N_s = N_1 \quad . \tag{A8}$$

But N_1, the noise contributed by the network, is equivalent to adding a noise $N_e = N_1/G_1$ at the input; i.e., N_e is the equivalent network noise, or in other words, N_e is N_1 referenced to the input terminals

of the network. Replacing N_1 by $G_1 N_e$, substituting $kT_s B$ for N_s and $kT_e B$ for N_e, and solving for T_e,

$$T_e = (F_1 - 1)\, T_s \tag{A9}$$

= equivalent network noise temperature referenced to the network input terminals.

The temperature T_s, which appears in this latter equation, is the temperature at the input to the network (see also Reference 15, p. 363). Present measurement standards require that the noise figure of receivers be measured with respect to an input termination at a reference temperature $T_0 = 290°K$. Thus, we replace T_s by T_0 to give

$$T_e = (F_1 - 1)\, T_0 \ , \tag{A10}$$

so that in terms of the equipment (or effective) noise temperature of the network, the noise factor becomes

$$F_1 = 1 + \frac{T_e}{T_0} \ . \tag{A11}$$

The concept of noise figure was originally formulated to describe the performance of relatively noisy receivers. The use of the noise figure with its standard temperature $T_0 = 290°K$ is not as convenient with low noise devices as is the effective (equivalent) system noise temperature. Although Figure A1 shows only one network, cascaded networks can be treated also. It can be shown (Reference 15, p. 364) that the noise figure F_0 for n cascaded networks is

$$F_0 = F_1 + \frac{F_2 - 1}{G_1} + \frac{F_3 - 1}{G_1 G_2} + \cdots + \frac{F_n - 1}{G_1 G_2 \cdots G_{n-1}} \ . \tag{A12}$$

Similarly, the effective noise temperature T_e of n networks in cascade is

$$T_e = T_1 + \frac{T_2}{G_1} + \frac{T_3}{G_1 G_2} + \cdots + \frac{T_n}{G_1 G_2 \cdots G_{n-1}} \ , \tag{A13}$$

or

$$T_e = (F_0 - 1)\, T_0 \ , \tag{A14}$$

where F_0 is given by Equation A12.

The noise factor F_0 and the corresponding T_e may be referenced to any point in the passive rf line system preceding the receiver. However, we have throughout this report been referencing the

noise temperature to the input terminals of the receiving system. Hence, we must also consider the effective noise temperature $T_{L,e}$ due to the rf line losses between the antenna and the receiver input terminals and the sky noise temperature T_{sky} due to background radiation (galactic noise, planetary noise, solar noise), sidelobe noise, backlobe noise, spill-over, and atmospheric attenuation. Since the sky noise is attenuated by the lossy rf line between the antenna and the receiver input terminals, then the effective sky noise temperature $T_{sky,e}$ referenced to the receiver input terminals is

$$T_{sky,e} = T_{sky}/L_R \quad , \tag{A15}$$

where L_R is the receiver line loss factor. In terms of L_R, the $T_{L,e}$ is given by (see Reference 28, p. 124)

$$T_{L,e} = T_L \left(1 - \frac{1}{L_R}\right) \quad , \tag{A16}$$

where T_L is the actual line temperature. Therefore, the total effective system noise temperature referenced to the input T_i becomes (see also Reference 28, pp. 124-125)

$$T_i = T_0 (F_0 - 1) + T_{sky,e} + T_{L,e} \quad . \tag{A17}$$

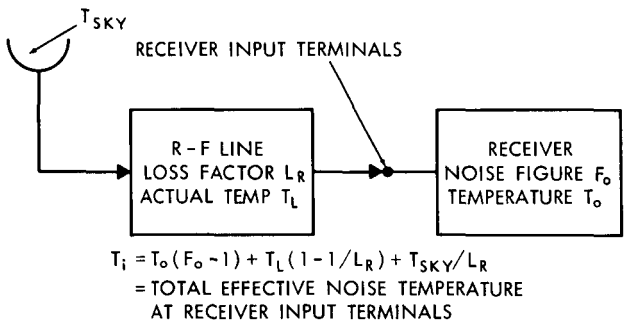

Figure A2—Receiver system.

Thus T_i is the temperature T to use in computing the total available noise power ($N = kTB$) referenced to the input terminals of the receiver (see Figure A2).

It should be noted that the effective noise temperature and the noise figure both describe the same property of the receiver. Controversy has existed over which is better. There seem to be, however, areas of usefulness for both definitions, and it is likely that they will both continue to be applied. The effective noise temperature is preferred for describing low-noise devices, and the noise figure is generally preferred for conventional receivers (Reference 15, p. 366). Furthermore, it should be noted that the effective noise temperature and noise figure are useful when dealing with systems which operate in the radio frequency spectrum, such as the microwave and millimeter wave systems, where $kT >> hf$ and thus the thermal noise predominates over the quantum noise. However, the effective system noise temperature is not useful in the optical spectrum, where $hf >> kT$, and thus the quantum noise predominates over the thermal noise. In the optical spectrum, the background noise and noise contributed by the detector are handled somewhat differently as demonstrated earlier in the text in the section on Mission Analysis where a laser ground beacon is detected by the spacecraft receiver in the presence of earth and reflected solar radiation.

Appendix B

The Point Ahead Angle

The point ahead angle (or lead angle) is the angle with which the optical beam must be pointed ahead of a target which is moving relative to the sources because of the finite amount of time it takes the signal to reach the target. As pointed out earlier, the point ahead angle must be controlled to within one part in up to about 300 (depending on the beamwidth and propagation time) because of earth and ground station motion relative to the spacecraft and the propagation times involved. More specifically, the earth orbital speed is approximately 30 km/sec. Since the spacecraft must first detect the ground beacon before pointing its own optical transmitter beam towards the ground, then the two-way propagation time should be used in this case to determine the point ahead or lead angle $(\theta_{\text{Lead Angle}})$. In addition the Bradley effect (sometimes called angle of aberration α) must be considered (see Reference 29, p. 379).

For simplicity, as shown in Figure B1, let t_1 be the time at which a bundle of photons is transmitted by the ground beacon; let t_2 be the time at which the spacecraft receives this bundle of photons; assume a negligible turn-around time, so that t_2 may be considered to be also the time at which the spacecraft transmits its bundle of photons towards the earth station; and let t_3 be the time at which the earth receives the downlink signal (i.e., the latter bundle of photons). Figure B1 also illustrates the Bradley effect. From Figure B1, it may be seen that in the spacecraft reference frame

$$\theta_{\text{Lead Angle}} \doteq \frac{S}{R} - \alpha \ , \qquad \text{(B1)}$$

where the negative sign is used before the α because of the convention adopted here that

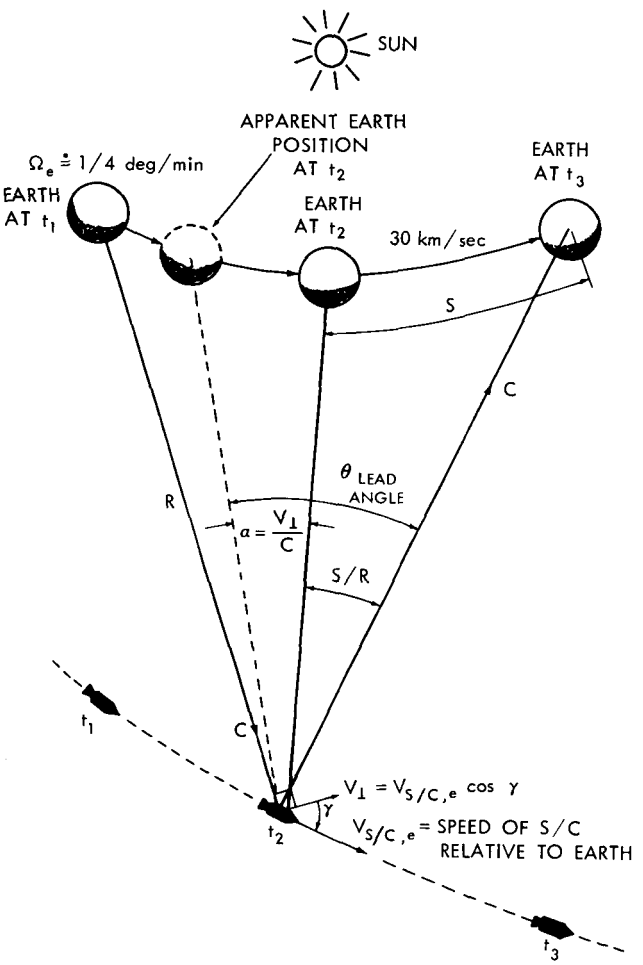

Figure B1—Geometry for computing lead angle.

velocity components are positive when directed along the positive direction of an axis, and angles are positive when measured in the counterclockwise direction. In any event, it is clear that one must be careful to give the proper sign to the angle α. From Figure B1, neglecting relativistic effects, the angle α is

$$|\alpha| \doteq \left|\frac{V_\perp}{c}\right| , \tag{B2}$$

$$V_\perp = V_{s/c,e} \cos\gamma , \tag{B3}$$

and

$V_{s/c,e}$ = speed of spacecraft relative to the earth station at time t_2.

The S is the distance (relative to the spacecraft) that the ground station has traveled normal to the line of sight (or the slant range R) during the one-way propagation time. Therefore

$$S = \left(\vec{\Omega}_e \times \vec{R}_e + \vec{V}_e + \vec{V}_{s/c}\right)_\perp t_{prop} = \left(\vec{V}_{e,s/c}\right)_\perp t_{prop} \tag{B4}$$

where

$\left(\vec{V}_{e,s/c}\right)_\perp$ = normal component of earth station velocity relative to the spacecraft and has the same magnitude as $V_\perp$ but is in the opposite direction,

$\vec{\Omega}_e$ = angular velocity of the earth's rotation on its axis with magnitude of ~1/4 deg/min,

$\vec{R}_e$ = station position vector relative to earth center with magnitude of ~6378.153 km,

$\vec{V}_e$ = earth's heliocentric orbital velocity with magnitude of ~30 km/sec,

$\vec{V}_{s/c}$ = spacecraft heliocentric velocity,

t_{prop} = R/c, one-way propagation time,

c = 3×10^5 km/sec, speed of light,

and hence

$$\frac{S}{R} = -\alpha \tag{B5}$$

At R = 1.852×10^8 km, t_{prop} is 617 seconds or about 10 minutes, and the two-way propagation time is about 20 minutes. Thus referring to Figure 1

$$S \doteq 11,700 \text{ km} ,$$

$$\left|\frac{S}{R}\right| \doteq 63 \ \mu\text{rad (a clockwise angle)} ,$$

$$\alpha \doteq \frac{V_{s/c,e} \cos\gamma}{c} ,$$

$$\doteq \frac{19 \text{ km/sec}}{3 \times 10^5 \frac{\text{km}}{\text{sec}}} \doteq 63 \ \mu\text{rad (a counterclockwise angle)} ,$$

when the spacecraft is in the vicinity of Mars (see Table 10 for typical values of $V_{s/c,e}$ and γ), so that

$$\theta_{\text{Lead Angle}} \doteq 126\ \mu\text{rad} \doteq 26\ \text{arc sec (a clockwise angle)} .$$

However, the beamwidth of the downlink at the half power points is

$$\theta_T \doteq \frac{\lambda_{co_2}}{d_T} \doteq \frac{10.6 \times 10^{-6}\ \text{m}}{1\ \text{m}}$$

$$\doteq 10.6\ \mu\text{rad} \doteq 2.2\ \text{arc sec}$$

for the downlink beamwidth being considered; the point ahead angle is 12 times larger than the beamwidth and must be controlled to within one part in 2×12 or 24 (3σ) as will be shown below. Since this point ahead angle is relative to the apparent line of sight of the received beam from the ground beacon, it appears likely that it should be possible to control it to within one part in 24 or about 1 arc seconds, because the point ahead or lead angle will be of the order of 26 arc seconds.

Since this point ahead angle is relative to the apparent line of sight of the beam received by the spacecraft from the ground beacon, then the accuracy with which it must be controlled is relative to this line of sight.

The beamwidth $(\theta_{\text{Beam Down}})$ of the spacecraft laser beam must be wide enough to assure that the ground station lies within this beamwidth at the time of arrival (t_3) of the bundle of photons transmitted from the spacecraft. Assuming a normal distribution,

$$\theta_{\text{Beam Down}} \doteq 2(3)\sqrt{\sigma_{\text{lead}}^2 + \sigma_{\text{point}}^2 + \sigma_{\text{LOS}}^2} , \qquad \text{(B6)}$$

where

σ_{lead} = one sigma error in the predicted lead angle,

σ_{point} = one sigma error in controlling the point ahead angle relative to the apparent line of sight,

and

σ_{LOS} = one sigma error in the apparent line of sight of the ground beacon beam received by the spacecraft and could be significantly less than 0.15 arc second (Reference 16).

The factor of 2 is used because the errors can be plus or minus, while the factor of 3 is used because the errors are one sigma and to assure a high probability (99.7 percent) that the ground station lies in the downlink beam.

Since $\vec{V}_e >> \vec{\Omega}_e \times \vec{R}_e$, then Equation B1 may be written as

$$\theta_{\text{Lead Angle}} \doteq \frac{2}{c}\left(\vec{V}_e + \vec{V}_{s/c}\right)_\perp = \frac{2V_\perp}{c} \tag{B7}$$

from which the uncertainty in the predicted lead angle is

$$\sigma_{\text{lead}} = \delta\theta_{\text{Lead Angle}} \approx \frac{2\delta V}{c} . \tag{B8}$$

Since the $\delta v_\perp$ may be expected to be of the order of meters per second, then this error as well as σ_{LOS} may be considered to be negligible, and

$$\theta_{\text{Beam Down}} \cong 2\left(3\sigma_{\text{point}}\right) . \tag{B9}$$

Hence, it may be concluded that the point ahead angle must be controlled to within half a beamwidth (3σ). For the case being considered here, the point ahead angle is 12 times larger than the beamwidth of 2.2 arc seconds, and hence must be controlled to within one part in 24 (3σ); i.e., to within ±1.1 arc second. Since this point ahead angle is relative to the apparent line of sight of the beam received by the spacecraft from the ground beacon, it appears likely that it should be possible to control it to within the required 1.1 arc second similar to what was done with a 3-ton gimbaled telescope on Stratoscope II (see Reference 16).

"The aeronautical and space activities of the United States shall be conducted so as to contribute . . . to the expansion of human knowledge of phenomena in the atmosphere and space. The Administration shall provide for the widest practicable and appropriate dissemination of information concerning its activities and the results thereof."

— NATIONAL AERONAUTICS AND SPACE ACT OF 1958

NASA SCIENTIFIC AND TECHNICAL PUBLICATIONS

TECHNICAL REPORTS: Scientific and technical information considered important, complete, and a lasting contribution to existing knowledge.

TECHNICAL NOTES: Information less broad in scope but nevertheless of importance as a contribution to existing knowledge.

TECHNICAL MEMORANDUMS: Information receiving limited distribution because of preliminary data, security classification, or other reasons.

CONTRACTOR REPORTS: Scientific and technical information generated under a NASA contract or grant and considered an important contribution to existing knowledge.

TECHNICAL TRANSLATIONS: Information published in a foreign language considered to merit NASA distribution in English.

SPECIAL PUBLICATIONS: Information derived from or of value to NASA activities. Publications include conference proceedings, monographs, data compilations, handbooks, sourcebooks, and special bibliographies.

TECHNOLOGY UTILIZATION PUBLICATIONS: Information on technology used by NASA that may be of particular interest in commercial and other non-aerospace applications. Publications include Tech Briefs, Technology Utilization Reports and Notes, and Technology Surveys.

Details on the availability of these publications may be obtained from:

SCIENTIFIC AND TECHNICAL INFORMATION DIVISION

NATIONAL AERONAUTICS AND SPACE ADMINISTRATION

Washington, D.C. 20546